SAPIENZA
UNIVERSITÀ DI ROMA

Motion Analysis and Control of Self-Assembled Sperm-Templated Micro-Bio-Robots

Dipartimento di Ingegneria Informatica, Automatica e Gestionale

Corso di Laurea Magistrale in Master in Artificial Intelligence and Robotics

Candidate

Jacopo Vivaldi
ID number 1823634

Thesis Advisors

Prof.ssa Marilena Vendittelli
Prof. Sarthak Misra

Co-Advisor

Dr. Islam S. M. Khalil

Academic Year 2019/2020

Thesis defended on 23 July 2020
in front of a Board of Examiners composed by:

Prof. Alessandro De Luca (chairman)
Prof. Aris Anagnostopoulos
Prof. Silvia Bonomi
Prof. Francesca Cuomo
Prof. Giuseppe De Giacomo
Prof. Domenico Lembo
Prof. Marilena Vendittelli

Motion Analysis and Control of Self-Assembled Sperm-Templated Micro-Bio-Robots
Master's thesis. Sapienza – University of Rome

© 2020 Jacopo Vivaldi. All rights reserved

This thesis has been typeset by LaTeX and the Sapthesis class.

Version: July 21, 2020

Author's email: vivaldi.1823634@studenti.uniroma1.it

Dedicated to my Mum

Abstract

The aim of this work is to investigate on the influence of the magnetization profile on the flagellar propulsion of a new micro-bio-robot called IRONsperm.
We introduce this hybrid device as the result of the electrostatic attraction between the negative charge provided by the body of a bovine sperm cell and the positive charge of ferromagnetic nanoparticles. The non-uniformity of the charge along the body of the sperm cell is such that the adhesion of the particles can vary from sample to sample.
We divided the body of the robot into four sections in order to identify 15 configurations, each characterized by a unique magnetization profile. In order to highlight the main features of the swimming behavior adopted by the different groups of IRONsperm, we approached the problem using two methods: an experimental analysis led to define the characterization of the frequency response within the range 1-20 Hz; the simulation of the motion through a mathematical model allowed to define the waveform pattern of each robot. Thanks to this inspection we concluded that the best configurations are the one identified as 0001 and 1100.
In this research, in terms of design and control, the combination of these results with important considerations taken during the analysis allows to make a considerable step forward that will contribute to the next phases of the project and will lead to adopt this new device for Cancer-relevant drug delivery.

Contents

1 Introduction **1**

2 Related Works **5**
2.1 Microrobotics 6
2.2 State-of-the-Art 9
2.3 Wireless Magnetic-Based Actuation 16

3 IRONsperm **19**
3.1 What is an IRONsperm? 20
3.2 IRONsperm Configurations: Magnetization Profile 24

4 Experimental Setup **29**
4.1 Octomag Inspiration 31
4.2 Helmholtz Setup 36
4.2.1 Helmholtz Coils 37
4.2.2 Feedback Systems and Computer Interface 42

5 Motion Analysis **45**
5.1 Characterization of the Frequency Response 47
5.2 Waveform Analysis 50
5.3 Trajectory Steering Control 55

6 Results **57**
6.1 Experimental Results 58
6.2 Theoretical Results 65
6.3 Discussion of the Results 77

7 Conclusion **83**

Bibliography **87**

Chapter 1

Introduction

In the most recent years, the microrobotics started to appeal the scientific community especially for the potentialities of its application in several fields. Robotics is often described as an interdisciplinary topic, and microrobotics takes this to another level [1] and it leads us to understanding many additional topics in physiscs, material science and biology. The development of this subject is strongly related to the progress of technology since, in order to obtain better performances and to extend the field of application of microrobotics, we need to consider novel technologies for the design of microrobots. The definition of microrobotics suggests that we are working at microscale and, at this scale, thanks to the studies of the most recent years, technology has been moving toward important improvements on the control of the biological components needed to design new hybrid devices. The main goal of microrobotics is certainly to provide effective tools for the exploration and exploitation of the microworld pushing the boundaries of this exploration from a robotics research perspective [20].

The control and design of microrobots imply a necessary understanding on how the physical effects change at microscale. This is fundamental in particular when we have to deal with the manipulation of biological cells. Many works, in the past years, were dedicated to the analysis of life of these cells at microscale. In particular, Purcell in "Life at Low Reynolds number" highlighted different aspects, from motion characteristics to physical features, of bacteria and other types of cells that fills the microworld that we cannot perceive.

The study of the physical effects is, of course, strongly related to the application field where micro-bio-devices have to be exploited to achieve the final goal. In particular, microrobots have the potential to revolutionize many aspects of medicine [3]. When we scale robots down to microscale, we need to understand how the physical effects such as viscosity and surface effects change. It is so important since this is the proper starting point for the development of medical microrobots. The influence of these factors combined with scaling issues that limit the fabrication lead to design wireless microrobots from a different perspective with respect to the traditional robotics one. This is challenging since we cannot take inspiration from macroscale and only experimental results allow to prove the efficiency of a

given microrobot design in a given application field. Medical microrobots must be designed to work in specific environments: the variation of size, geometry and material properties in these environments makes the procedures very tricky. In fact, designing a single microrobot that is able to negotiate changing environments is not trivial [23].

As explained, the design of functional microrobots in the medical field is challenging from an engineering point of view, but the potentialities are really vast. This is why, in this work, we focus on the description of the design of a new hybrid microrobot and on the analysis of its motion in order to highlight the main features that allow to improve the performance of this device.

This work reports the several steps and the main aspects that my thesis project involved in. In particular, we proceed by presenting the state of the art in medical microrobotics and specifically we include the description of relevant models that can be seen as the ancestors of our new micro-bio-robot.

The name of this new hybrid device is IRONsperm. The studies conducted by Magdanz et al. in [20] investigated on the charge distribution of bull sperm cells. Their findings suggest that the charge distribution of the sperm membrane is not uniform and it presents an overall negative net charge. Assuming these considerations, the electrostatic attraction between the negatively charge dead sperm cell bodies and positive nanoparticles allowed to create our new micro-bio-robot. The ferromagnetic particles applied on the body provide magnetic dipole moments under the application of an external magnetic field used to control both the propulsion and the direction of the robot.

This project comes out from the collaboration of the Surgical Robotics Laboratory of University of Twente with the Technical University of Dresden, Sapienza University of Rome, German University in Cairo and University Medical Center of Groningen. Thanks to these collaborations I had the chance to work at Surgical Robotics Laboratory with Dr. Islam Khalil and Prof. Sarthak Misra, who are experts in the world of microrobotics and, in particular, in its application in the medical field. This experience gave me the opportunity to work with Dr. Veronika Magdanz, who gave one of most important contribution to this project. This thesis reports only the first of a bigger project whose aim is to design and control the IRONsperm in order to use it for localized drug delivery. In this context, the goal of this application is to succeed to use these devices to treat cancer cells. It was already tested in [27] that cellular micromotors, in particular sperm cells, can be used for delivering high concentrations of drug and targeting hard-to-reach disease sites such as cervical cancer [27].

It was already proven that spermatozoa can work as highly efficient microrrmotors for drug delivery in different environment inside the human body. In this thesis we want to investigate on the influence of the magnetization profile on the flagellar propulsion of the IRONsperm. To achieve this goal we proceeded with the analysis of the motion of the IRONsperm in order to highlight the main features that we want to take advantage of for the next phases of the project.

In the following chapters, we will present the details of the design of the robot. After this we will describe the main characteristic of the experimental setup that is kept at Surgical Robotics Laboratory. This setup provides the electromagnetic system needed to properly actuate the hybrid devices and the microscopic system used to localize it during in vitro applications. The analysis of the motion will be defined under two different point of views: the first approach is an experimental procedure that implies extracting the characterization of the frequency response for each configuration of the IRONsperm in a given frequency range; the second approach is based on the simulation of the motion using a numerical model. It leads to define the wave propulsion for all the configurations of the IRONsperm.

The combination and the comparison of the mentioned methods are expected to return which are the configurations to discard and, instead, which are the configurations to keep and to work on during the next phases of the projects. This analysis is expected to highlight the main features of the IRONsperm that we want to focus on for design purposes, whereas, different procedures adopted during the experimental analysis gave the opportunity to make considerations on a future adoption of a control approach. This analysis will provide a strong base for the next steps of the project, and all these elements will allow to accomplish the localized drug delivery for treating cancer cells using IRONsperm.

Chapter 2

Related Works

The aim of this chapter is to illustrate and provide examples of the potentialities of the microrobots. The recent studies on these new kind of robots are developing a new set of devices and techniques that are expected to revolutionize different aspects in many research fields.

In particular, during the first part of this work, we will recall the state-of-the-art of micorobotics, starting from the very first years of research. We will give an overview on how these devices were analyzed and developed over the years and we will focus on the aspects that can allow to introduce the new micro-bio-robot that was created in this project. In fact, after a presentation on the main aspects that characterize the design and control procedures of these robots, we will focus on how to use them in the medical field. These devices have the potentialities to deeply improve many aspects of medicine. For example, these untethered, wirelessly controlled and powered devices will make existing therapeutic and diagnostic procedures less invasive and will enable new procedures never before possible [23].

We want to explore the potential impact of the application of microrobots in medical field. This in-depth analysis is supposed to provide valuable information to prepare the reader to the next sections of this work. The examples that we are providing to illustrate the manipulation of sperm cells in microrobotics are strongly related to our project. In fact, we will explain how our new device takes inspiration from many characteristics previously defined for other robots. These engineering tools are needed for the design of medical microrobots to inspire future research in this field. This is why all these points, from the design aspects to the control procedure, provide a strong base to understand our work and the features of the IRONsperm that will be presented in the next chapter.

2.1 Microrobotics

In 1950s, the introduction of new integrated circuit manufacturing techniques pushed toward realizing smaller and smaller electrical and mechanical components. It led to the birth of a new field in robotics called microrobotics. The term "microrobotics" is meant to define robotic devices and manipulation techniques in the millimeter to micrometer range. In those years, biologist and physicists started to approach to study how microorganisms as bacteria and spermatozoa proper themselves. From that moment, scientists looked at the nature as a source of inspiration for the microrobotics designs, but only in the 1990s the robotics community started to get interested in microscale.

Microrobotics is not only about the design and fabrications of robotic agents in a scaled size range. In fact, it includes also micromanipulation, but the scaling of physical effects makes even the simplest manipulation tasks challenging. The microscopic world is governed by the same physical laws as the macroscopic world but the relative importance of the physical laws changes. Fluid viscosity and surface effects such as electrostatics dominate over volumetric effects such as weight and inertia, and the generation and storage of power becomes difficult [23]. The scaling of electromagnetic forces and adhesion forces are both of particular interest in the field of manipulation of microrobots. In particular, the first ones are of great interest when a system able to propel a microrobot agent wirelessly through the use of a magnetic field.

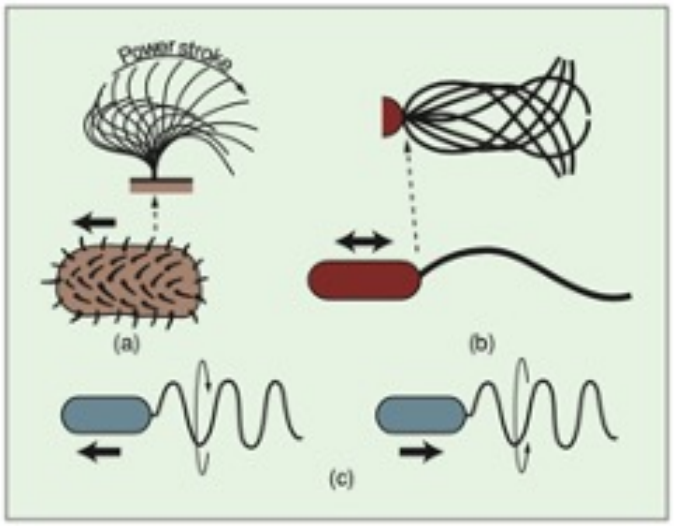

Figure 2.1.
Locomotion of microrganisms: (a) Cilia moving across the flow; (b) Eukaryotic flagella swimming pattern; (c) Molecular motor spin bacterial flagella.

One of the most important applications for microrobotics is the biological cells manipulation. In fact, generally animal cells size is between 1 and 100 μm and then microrobotics tools are needed to manipulate single cells. The use of microrobotics for controlling biological cells led to the introduction of these techniques into the medical field, in particular into the minimally invasive surgery.

Microrobots can be used by a surgeon for simple functions that allow to accomplish different tasks. In the following figure, it is possible to appreciate a classification of the main applications of the microrobotics in medicine that prove the potentialities of the microrobots to perform medical procedures throughout the human body. It is important to highlight the fact that in many of these applications the accomplishment of goals through the use of microrobots can be achieved only under the supervision or the teleoperation of a clinician.

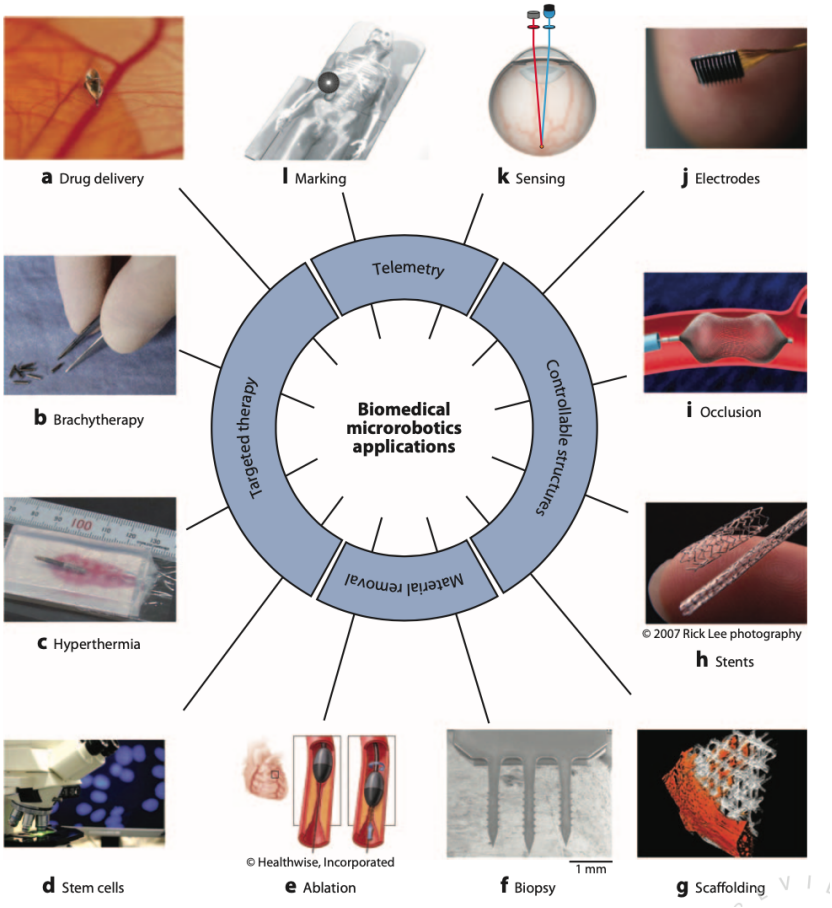

Figure 2.2. Microrobotics in MIS: Application Areas.

Since the large number of application areas for medical microrobots, the study of different types of design created a great interest. In particular, inspired by eukaryotic flagella, a number of microswimmer designs use a form of travelling wave to generate propulsion for locomotion. In particular, several researchers focused on the development of a hybrid bio devices able to exploit the characteristics of a

natural sperm cells to achieve different medical tasks.

Figure 2.3. Travelling wave propulsion with an elastic tail.

In the next section, we are going to show some examples of the microrobots agents that were used as inspiration for the work illustrated in this thesis. In particular, we will focus on hybrid microbiorobots that exploit sperm cells since they offer the possibility to navigate through the fluids of the human body as they are not toxic [10].

2.2 State-of-the-Art

As mentioned in the previous sections, the physical effects change when we analyze the microscopic world. This latter is governed by the same physical laws as the macroscopic world but the relative importance changes. This is why we need to deeply study the new physical dynamics that we can encounter. In particular, for this project it is fundamental to understand the fluid mechanics in order to evaluate the behavior of the micro-bio-robot. As explained in [1], the Navier- Stokes equations, when combined with appropriate boundary conditions, completely define a fluid's velocity in space and time (assuming that there is no phase transition). For an incompressible fluid with constant viscosity, they are given by the vector equation:

$$\rho \frac{dV}{dt} = -\nabla p + \eta \nabla^2 V$$

where V is the velocity vector field, p is the hydrodynamic pressure scalar field and ρ and η are the fluid's constant density and viscosity, respectively [1].

This equation is important because it allows to derive the Reynold number, that is a dimensionless quantity that embodies the interaction between a fluid's inertia and viscosity as it flows around an object [1]. Assuming that V_s is the magnitude of a free-stream velocity and L is the characteristic length of the object of interest (e.g. the lenght of the sperm cell flagellum), then we can derive the formulation of the Reynolds number:

$$Re = \frac{\rho V_s L}{\eta}$$

Generally, we are used to think about the behavior of a liquid with high Re, but at low Re, we are in a world that is either very viscous, very slow, or most importantly for our present discussion, very small. At low Re it is possible to neglect some terms in the fluid and the equation that governs the fluid behavior becomes:

$$\tilde{\nabla} \tilde{p} \approx \tilde{\nabla}^2 \tilde{V}$$

The flow pattern does not change considerably, and the flow is reversible. This is described by the fact that the time no longer appears in the equation.

Purcell says that this is "a world we almost never think about" and it is "quite different from the one that we have developed in our intuitions in". His famous work "Life at low Reynolds number" provide the basis for the analysis and the development of a microrobot design.

Here, he investigated on the behavior of fluids characterized by a low Re and on the swimming patterns that different microorganisms adopt to move. Since these mechanisms are not time reversible then they lead to a net translation since inertial effects are not considered. Purcell recognized three main swimming mechanisms: the "coreskrew", a swimming behavior adopted by many bacteria where a rigid helical filament is rotated in a viscous fluid; "three-link swimmer", a simple and

rigid mechanisms to swim without inertia; and, finally, the “flexible oar”, where travelling waves are generated along the flexible tail that produces propulsive force by oscillating in a viscous fluid.

The latter is the mechanisms that we are interested in in this work. As Yu et al. has reported in [29], presenting an experimental investigation of this propulsive mechanism by constructing a robotic swimmer able to provide propulsive force using the tail elasticity, we want to analyze in detail the motion behavior in a fluid at low Re of our new hybrid device. Traveling waves are more efficient than helical propellers since they can produce an effective means of propulsion in a fluid at Low Reynolds number, but only if the actuation is well distributed.

In the state of the art, different microrobotics designs able to provide propulsive force using the tail have been proposed since it was noted that one of the most successful actuation methods for this goal is to take advantage of the natural elasticity of the cell body. Planar flagellar propulsion have been studied by Khalil et al. in [15] where they developed “a magnetically driven soft two tailed microrobot capable of reversing its swimming direction without making a U-turn trajectory or actively modifying the direction of wave propagation”. The peculiarity of this design is that it presents two collinear, unequal, ultrathin tails: one tail provides propulsion below one of the reversal frequencies and the other one is passive; viceversa, in the opposite direction the second tail provides propulsion above the reversal frequency and the first one is passive.

During the recent years, a significant interest in exploiting motile sperm cells grew up in order to achieve locomotion and propel microobjects in viscous environments. In fact, the combination of synthetic micro- and nanomaterials with spermatozoa as functional components has led to the development of new microrobotic designs with potential applications in the biomedical and nanotechnological field [21]. In order to integrate these cells as active components for new designs of microrobots, their biological and dynamic characteristics, such as the influence of temperature and viscosity on their behavior, have been studied such that their optimum functions can be ensured. Their application in the biomedical field is promising since they can be both used as actuators and as cargo to be delivered in a region of interest, such as the fertilization site in an artificial insemination operation.

As we mentioned before, the final aim of this project is to design and control a microrobot for localized drug delivery. As we will see in the next sections of this work, also our microrobot use as biological part the natural sperm cell. Medina-Sanchez et al. in [10], proved the efficiency of these cells for cargo delivery also in in vivo applications. In [28], Xu et al. developed a similar system for localized drug delivery aimed to treat diseases in the female reproductive tract. In the following figure, we can appreciate the process of loading a motile sperm cell with doxorubicin hydrochloride , that is an anticancer drug.

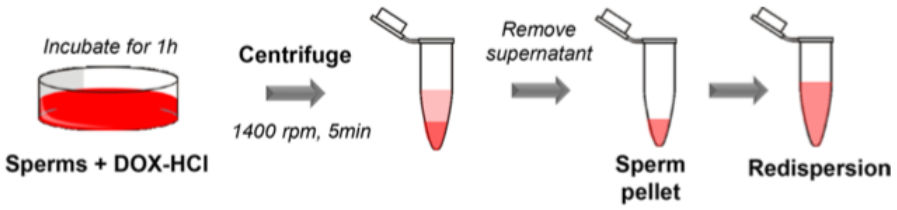

Figure 2.4. Experimental flowchart for loading DOX-HCI into sperms.

Recently, the biotechnology community focused on the development of micromotors that can be biocompatible with functional components, like sperm cells, for in vivo applications. For example, in [22] the microrobots are used for assisted fertilization and customized microhelics are used as artificial micromotors for transporting sperm cells with motion deficiencies. Similarly, Magdanz et al. in [18] focused on the design of polymeric microtubes: the sperm cells are captured inside these tubes and then they can be transported and remotely controlled to achieve the desired final task.

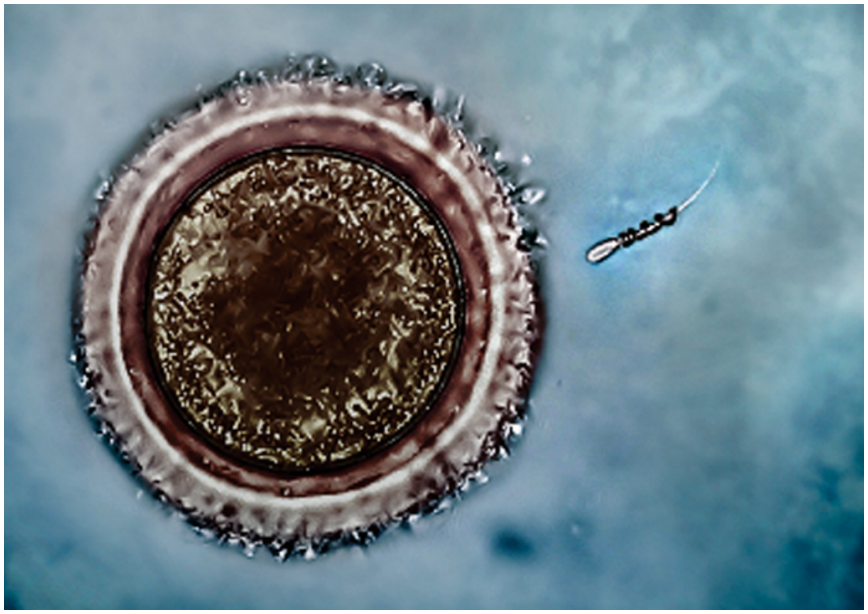

Figure 2.5. Sperm-Carrying Micromotors.

These recent studies led to develop a new class of micro-bio-robots (MBR) as hybrid devices where the biological functional part is constituted by the sperm cell and the artificial part is generally a micro-tool that can be attached to the cell in order to allow the remote control of the device. In fact, a microrobot can be controlled wirelessly using an external magnetic field and it can be oriented along the direction of the magnetic field and pulled by the gradients in that field. This strategy is used to mimic swimming methods of microorganisms and hence it can induce a wave motion in the tail without on board actuation.

In the state of the art, the magnetic actuation of microrobots has been studied. We can distinguish mainly two different categories of microrobots: artificial microrobots, that does not include any biological part in the design; hybrid microrobots, that are a combination of the advantages offered from the artificial microstructures and the natural characteristics of the cell. In [11], Khalil et al. investigated on magnetic-based motion control of a sperm-flagella driven micro-bio-robots and they proved point-to-point closed-loop motion control under the oscillation of an external magnetic field.

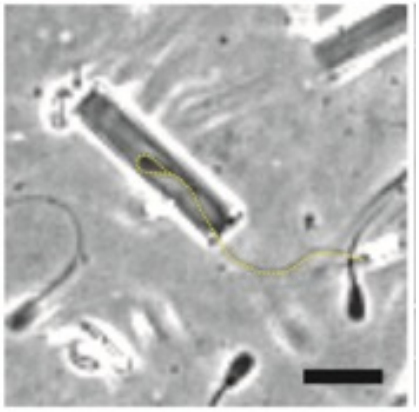

Figure 2.6.
Sperm-driven Micro-Bio-Robot consisting of a microtube and a bovine sperm cell.

In [10], Khalil et al. developed a bio-hybrid microrobot by capturing a single sperm cell in an artificial magnetic microstructures. This device is called "Spermbot" and its motion is generated by the coupling of the cell and magnetic structure: in fact, the first imparts propulsive force to swim, whereas the microtube made of 3D maskless lithography provides a magnetic dipole moment for directional control under the influence of an external magnetic field. For this kind of devices the interaction with the external magnetic field and with the viscous fluid where it swims in have been tested and directional control under magnetic field and sperm-mediated drug deliveries have been demonstrated.

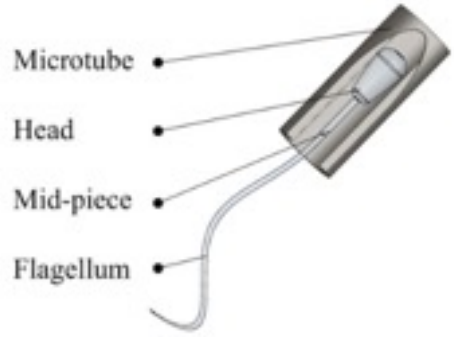

Figure 2.7. Spermbot design scheme.

Differently from the Spermbot, now we are going to show an example of a totally artificial microrobot developed in [12] .

This artificial structure is called “MagnetoSperm” and its motion is similar to the propulsion provided by a natural sperm cell. The design of this new device is realized through a chemical process simplified in the proposed image. The two main aspect to highlight are the attempt to reproduce the natural elasticity of the tail and application of a magnetic layer of cobalt-nickel to the ellipsoid head of the sperm-like structure. The use of this material provides a dipole moment such that the robot can align along the direction of the soft magnetic field and generating a propulsion thrust force that overcomes the drag force. With respect to the Spermbot where we controlled only the direction of the robot, here we are using external actuation both for propulsion and direction.

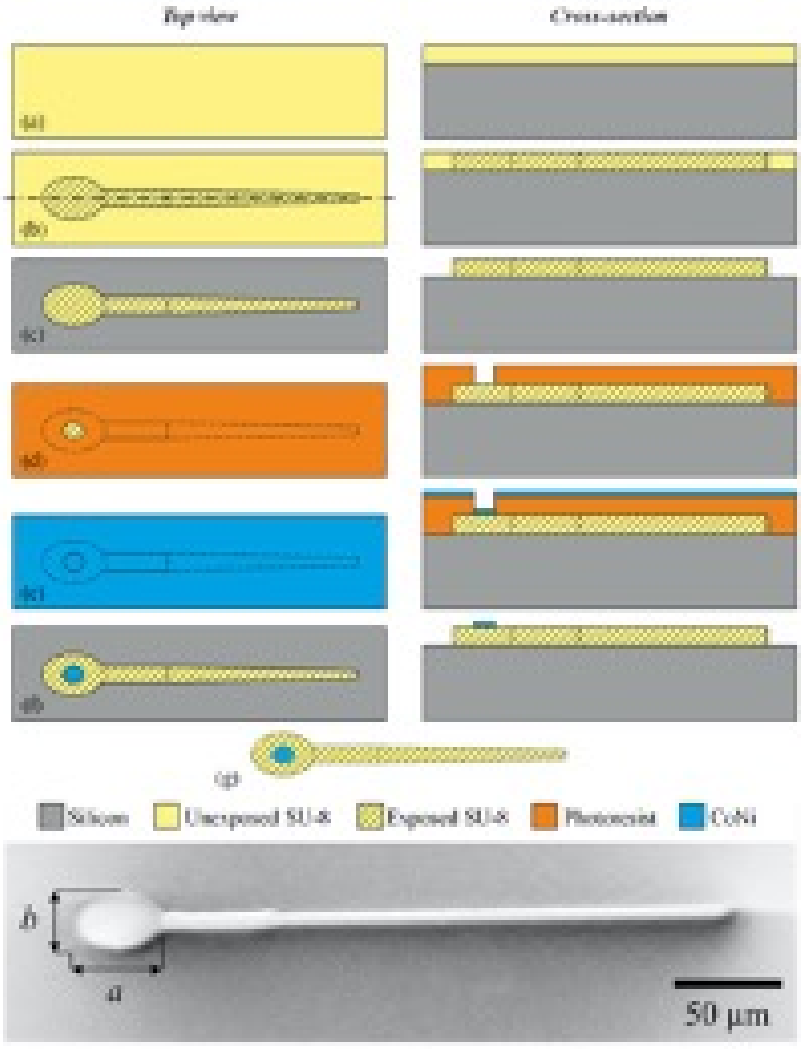

Figure 2.8. Schematic illustration of the fabrication of MagnetoSperm.

In the light of the illustrated progresses obtained in the microrobotics field, we are going to show our novel device able to swim in a viscous fluid under the actuation of a weak external oscillating magnetic field.

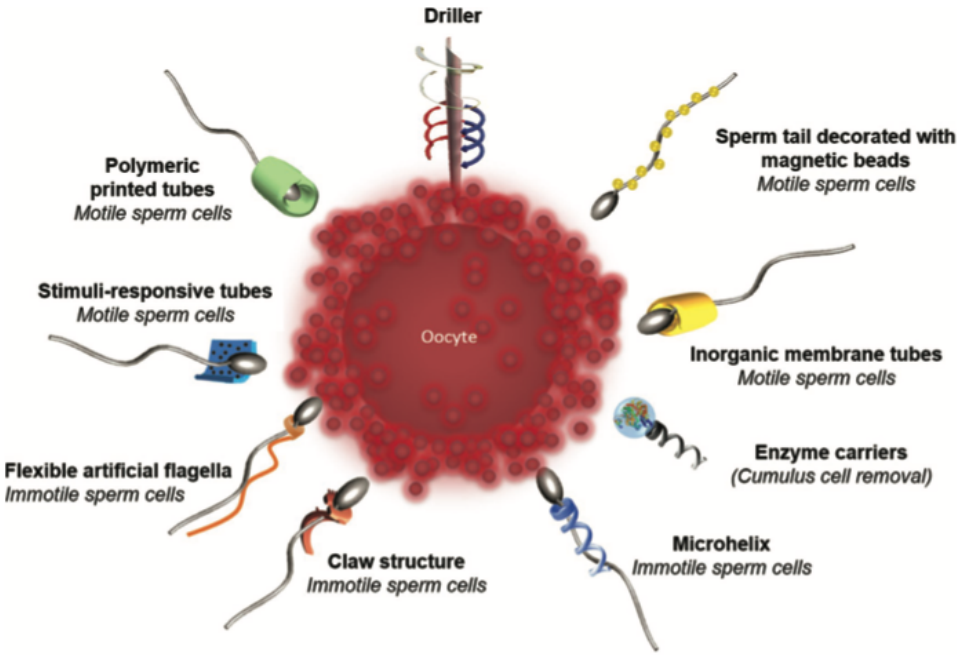

Figure 2.9. Novel microswimmers design for targeting fertilization.

2.3 Wireless Magnetic-Based Actuation

Any robotic device needs accurate techniques for the spatial and temporal control of their actuation. Ideally, these control techniques should be in a remote and biocompatible manner and without time loss [21].
Flexible artificial microswimmers were fabricated using several procedures and methods in order to produce different designs which allow their remote actuation by an external magnetic field. In particular, for microrobots that uses spermatozoa as functional components, this strategy allows to obtain a sperm-like motion of the flexible microrobots.

The actuation method generally consists in generating an oscillating magnetic field that, thanks to the characteristics of the design of the microrobot, causes the body of the sperm robots to fluctuate. The application of the magnetic field can be used both to actuate the microrobot and to only steer it. This control strategy is interesting in the field of microrobotics, since the wireless pulling through the use of field gradients is not possible for autonomous microorganisms and then there is not any analogy with nature. For this reason, "it is reasonable to conjecture that it might provide a more effective means of wireless propulsion than anything that could evolve through natural selection" . This conclusion leads to an interesting consideration: as we explained at the beginning of this chapter, the study for conceiving the design of microrobots started from taking inspiration from the nature and now, thanks for the progresses of technologies and techniques, we are approaching to overcome the strenght of the nature on different aspects.

Controlled magnetic fields can be generated in several ways. One of the most common method is use electromagnets that can be simultaneously position and current controlled. For example, Yesin et al. in [28] have developed an experimental setup that uses a pair of electromagnetic coils to superimpose a uniform field with the gradient field produced by another pair of coils.
One of the most famous prototypes for this remote control strategy is the OctoMag presented in [17]. This work demonstrate the efficiency of a five degrees of freedom wireless magnetic control for a fully untethered microrobot with two degrees of freedom for the position and one degree of freedom for the orientation. This setup is very interesting in our work since the experimental setup developed in the Surgical Robotics Laboratory at University of Twente took inspiration from this model. The primary application of this system was to control intraocular microrobots during retinal procedures, even though, this design presents many potential applications in the medical field.

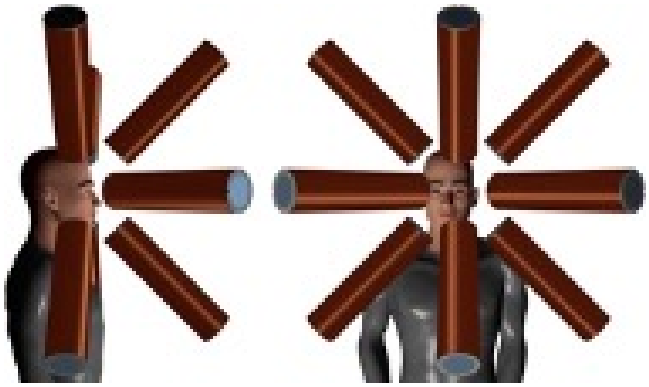

Figure 2.10.
Assuming an eyeball at the center of the workspace, this simulated scheme shows the system for the control of intraocular microrobots.

The design of OctoMag follows four main guidelines:

1. Electromagnets are stationary to ensure safety.
2. The design has to respect the geometry of the human head (due to its primary application).
3. A larger prototype was built to test in vivo applications on animals.
4. The workspace should be isotropic such that there is the possibility to apply the magnetic forces in any direction with any microrobot pose.

Figure 2.11. OctoMag prototype at ETH Zurich.

The main challenge of this system is to perform 5-DOF wireless control of microrobot in a stationary world frame of reference, and to define a design procedure that allowed to maximize the control performances for many kinds of applications that

involves different electromagnetic configurations.

A similar approach was used in Khalil et Al. [16] to demonstrate precise closed-loop control of microjets, where the combination of the self-propulsion and the magnetic control allows the microrobot to move in 3D space and then to move also upward and downward in the viscous fluid.

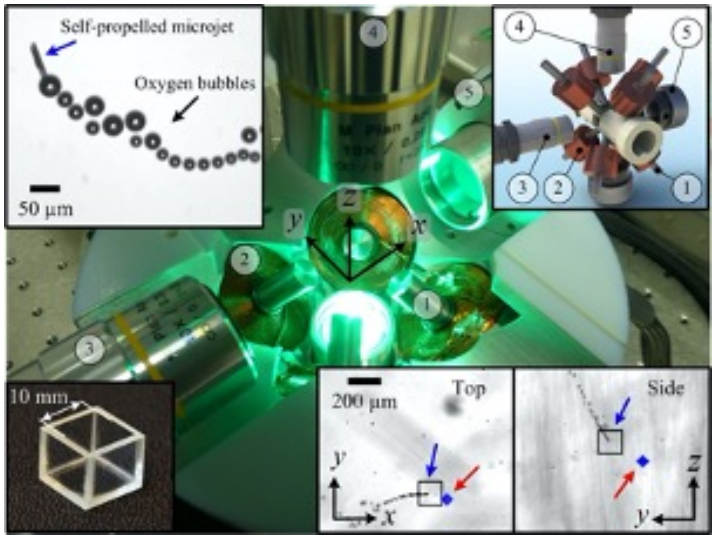

Figure 2.12.
Electromagnetic system for the wireless control of microjets in three-dimensional space.

Thanks to these studies in the recent years, it was demonstrated how magnetic fields can be introduced to help mimic swimming methods of microagents without using onboard actuation systems. This control approach allows to define actuation strategies that has no direct analogy in nature, and then they are not possible to be performed by natural autonomous microorganisms. Pulling with magnetic field gradients, besides actuation approaches that uses magnetically driven helical propulsion or magnetically driven elastic tail propulsion, have shown promising results for medical applications.

These wireless magnetic-based control systems have many potentialities: they can be used to control magnetic forces and torques on microagents, as we have seen in the previous examples, but also on magnetically tipped catheters and guidewires. The control of microrobots through the use of these systems can allow targeted delivery of small quantities of concentrated drugs. The final aim of this project is exactly to find a strategy to use IRONsperm to deliver drugs in a region of interest, and t now it is clear why we are going to use a wireless magnetic-based manipulation system.

Chapter 3

IRONsperm

As mentioned in the previous sections, recent studies have confirmed the potential of introducing spermatozoa as functional parts of a hybrid microrobot for biomedical applications. These potentialities derive from the different advantages that these biological cells provide. Swimming at low Re means simply that you are in some liquid and are allowed to deform your body in some manner [24]. The spermatozoa are able to propel themselves and control the flow field in a viscosity-dominated flow regime thanks to the transverse waves along their self-propelling undulatory systems. This undulatory system is of particular interest to achieve controlled actuation based on an external stimuli. Moreover, we highlighted how the sperm cells can be efficiently used for cargo delivery: this is a necessary characteristic for our micro-bio-robot since the final aim of this project is to develop a system that allows to control the IRONsperm for drug delivery in a region of interest.

In the previous section, we explained how the robotics and biotechnology community investigated on how to design new hybrid devices combining spermatozoa with artificial magnetic tools that allow to achieve controlled actuation based on external inputs as the application of an external magnetic field. Moreover, we commented different devices, presented in the state of the art, that use as main approach to construct a self-propelling undulatory system the integration of a motile microorganism to a magnetic constituent [14].

Hybrid bio devices are preferable with respect to artificial swimmers since the natural optimal design and elasticity of the natural microorganisms are a desirable properties that allow to obtain better performances. The motion control strategy of these hybrid devices relies on the propulsive force of the motile sperm cell, whereas, it exploits the effects produced by the application of the external magnetic field to control only the direction of the robot. In this section, we are going to see the details of the design of this hybrid robot and how we took advantage of the magnetic interaction to produce the motion of the IRONsperm inside the fluid.

3.1 What is an IRONsperm?

In this work, we present a novel device that combines sperm cells elasticity with magnetic actuation both for propulsion and directional control. For this new design the surface charge of the cell plays a fundamental role on the determination of the magnetization profile of the sperm-templated micro-bio-robots.
Magdanz et al. in [20] have proved that bovine sperm cells present non-uniform charge distribution and negative overall net charge. This study led us to the development of a new Hybrid bio microrobot device called "IRONsperm": this design merged out from the combination of immotile sperm cells and rice grain shaped particles. Dead bull sperm cells, as mentioned before, are characterized by negative and non-uniform charge along their body, then the negatively charged location is coated with particles that are naturally ferromagnetic and then positively charged.

The generation of these devices must follow the protocol presented below:

1. **Take 1 mL of boar sperm suspension.**
2. **Centrifuge:**

   8000 rcf for 5 minutes
3. **Remove supernatant:**

   After the centrifuge all the sperm cells are concentrated on the bottom of the test tube. Use a pipette to remove all the rest of the liquid without touching the sperm cells concentration.
4. **Add 1 mL of H2O:**

   When you add water, pull it up and down to remove the suspension and start mixing the solution.
5. **Mix well:**

   Use the vortex mixer.
6. **Add 50 μl of nanoparticles**
7. **Leave overnight in the fridge:**

   You do not need to keep the sperm cells alive, so you can use a normal fridge. (If you need to keep them alive use the biology laboratory fridge that is set to 16°C).
8. **Expose to permanent magnet for one minute.**

Each step of this protocol must be carefully followed in order to ensure the correct generation of new samples of IRONsperm. Anyway, this protocol is specially made for bull sperm cells: in fact, it was tested for boar sperm cells too, but their different surface charge prevents from generating the desired hybrid devices since the rice particles do not attach to the sperm flagellum.

The following image shows a schematic of the IRONsperm such that we can introduce the notation for the formalization of the hybrid micro-bio-robot motion model:

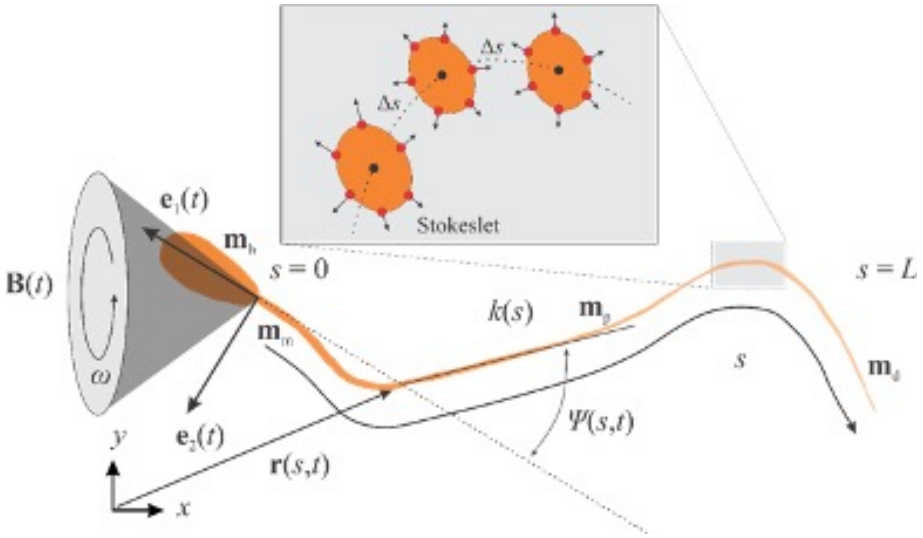

Figure 3.1. Schematic of a hybrid micro-bio-robot with axial length L.

The arc length s is equal to 0 at the head position and it is equal to L, the length of the sperm cell, at end of the tail. The flagellum is characterized by the tangent angle $\Psi(s,t)$, as a function of the arc length s, measured between a fixed frame of reference $e_1(t)$ and the local tangent at position $r(s,t)$ along the flagellum.
We consider four segments along the sperm cell respectively defined as the head, the mid-piece, the principal piece and the distal end. In this scheme, we define average magnetic moments m_h, m_m, m_p, and m_d that corresponds respectively to the head, the mid-piece, the principle piece, and the distal end. These magnetic moments are provided to the organic body by the magnetite nanoparticles, and the resulting micro-bio-robot is externally actuated by a periodic magnetic field $B(t)$. This latter is constrained to a finite steradian with cone angle α and its frequency ω can vary.

The wave propulsion that produces motion for these microrobots derives from the deformation of the tail. In fact, the magnetic toque exerted on the flexible flagellum, of bending stiffness of $\kappa(s)$ generates a traveling bending wave that is ultimately responsible for the flagellar swim [14].
The micro-bio-robot is immersed in an inertialess viscous medium, characterized my low-Re, and lies in an external magnetic field $B(t)$. In low-Re, the fluid drag force is a linear function of the velocity ($\xi_{n_i} \frac{\delta \Psi}{\delta t}$), opposing the restoring force ($\kappa_i \frac{\delta^4 \Psi}{\delta s^4}$) of the flagellum. ξ_n and κ are the normal drag coefficient and bending stiffness of the flagellum, respectively. Magnetic bending moments ($M(s)$) are applied at the positions of the nanoparticles. Therefore, the governing equation is given by:

The following relation expresses the balance between hydrodynamic drag exerted on each segment and magneto-elastic coupling between the nanoparticles and these

segments:

$$\kappa_i \frac{\delta^4 \Psi_i}{\delta s_i^4}(s_i, t) + \xi_{n_i} \frac{\delta \Psi_i}{\delta t}(s_i, t) = \sum_i \frac{\delta^2 M_i(s)}{\delta s^2} \quad i = h, m, p, d$$

This equation expresses the balance between the drag and the elastic forces exerting on the flagellum of the IRONsperm and the magnetic moments activated by the application of the external magnetic field. The first term of the equation is composed by two elements: one is the magneto elastic coupling between the nanoparticles and the segments of the body of the sperm cell. This term tends to restore the flagellum to its original natural shape. The second one indicates the hydrodynamic drag exerted by the fluid on each segment of the body of the cell. The second term of the equation provide the magnetic moments produced by the nanoparticles that adhere on the body of the dead sperm cell. This element is equal to zero when the external magnetic field is not activated or there are no particles on the body of the cells. Contrarily, it becomes different from zero when a magnetic moment is activated by the actuation of the external magnetic field. Since the distribution of the particles is not uniform along the cell then we obtain a non-uniform distributed actuation for each magnetization profile. IRONSperms are driven by the bending moments applied by the external magnetic field at the location of the nanoparticle aggregates and they induce a traveling wave that propagates from the head to the distal end, producing a net thrust force that propels IRONSperm forward.

In order to model the actuation, we need to specify boundary conditions for each segment and then we can start predicting the response of the microrobot. This latter and, consequently, the propulsion of the IRONsperm is predicted using the method of regularized Stokeslets for computing Stokes flows. In fact, as we previously mentioned, when we use a viscous fluid characterized by a low Reynolds number, then time no longer appears in the equation that governs the flow. It means that the flow is reversible and a "low-Re flow around a body is referred to as a creeping flow or Stokes' flow" [1].

The Stokes' law is valid for at least $Re < 1$ and it expresses that the viscous drag force on a sphere with a given diameter d in an infinite extent of fluid can be defined as a linear function of the sphere's velocity through the fluid:

$$F_{drag} = 3\pi\eta d V_s$$

The meaning behind this equation is that the shape of the body lose importance when the Reynolds number is reduced and then the Stokes' law becomes a good predictor of drag force on different shapes.
Stokeslets are defined as the solutions of the Stokes' law and the method of regularized Stokeslets is a numerical Lagrangian method to compute Stokes flows driven by forces distributed at material points in a fluid and in presence of immersed boundaries [2, 3].

The inset of figure 3.1 shows that the surface of flagellum can be decomposed

into Stokeslet points with Δs between the points. This decomposition allows to derive the velocity of nearly 100 Stokeslet points: in fact, using the Resistive Force Theory, as we did at the end of this work, it is possibile to provide the force of the flagellar propulsion. This result can be combined with the Stoke's Law in order to produce the expected velocity field given the force acting on a point along the flagelluum.

3.2 IRONsperm Configurations: Magnetization Profile

According to the mathematical model presented in the previous sections, we started to study the magnetic-based motion control for a Micro-bio-robot (MBR) like the IRONsperm and, indeed, how it is influenced by the application of an external rotating magnetic field. This hybrid device is an example of how the development of microrobots able to be wirelessly controlled can be achieved by the implying biological motors, also using non-motile micro-organism or cell.

Before of starting to analyze the features that characterize the motion and the propulsion of this microrobot, We want to present the properties of magnetically actuated passive flagella of dead sperm. In particular, in this section, we are going to focus on the categorization that we adopted in order to distinguish 15 different configurations of the same robot. This work investigates on the dynamic behavior of groups of hybrid micro-bio-robots with various magnetization profiles [14] that depend on the spatial distribution of the nanoparticles along the body of the sperm cell.

Since the bovine sperm cells present the characteristic to have a non-uniform charge distribution, and negative overall net charge, we expect that, if we coat the negatively charged locations along the cells with positively charged particles, then it could lead to selectively magnetize various segments of the sperm cell body. This is the principle which our categorization of the IRONsperm is based on.
As shown in the following figure, in order to distinguish the different configurations, we had to divide the sperm cell body into four sections: head, mid-piece, principal piece and distal end.

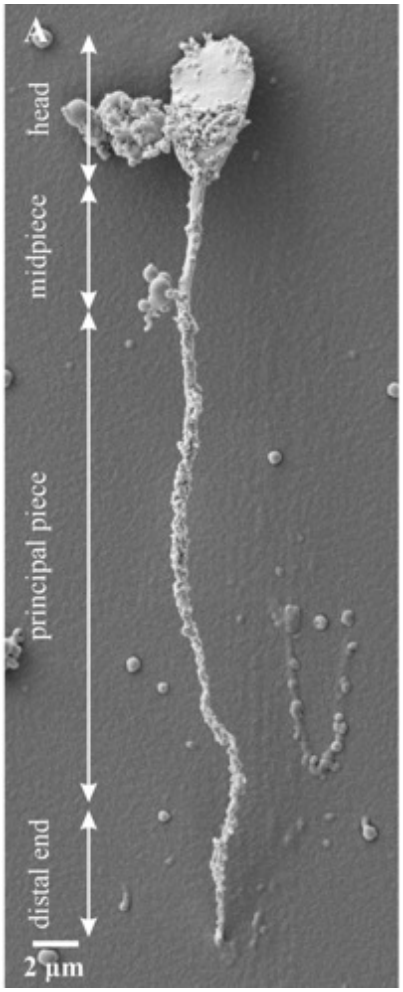

Figure 3.2. IRONsperm sections: head, mid-piece, principal piece, distal end.

This scheme allows to appreciate in detail how the magnetic aggregation between positively charged nanoparticles and negatively charged sperm body can result in the new robot that we call IRONsperm.

In the figure 3.3, we can see how rice-grain shaped nanoparticles (NPs) can adhere to different segments along the sperm cell.

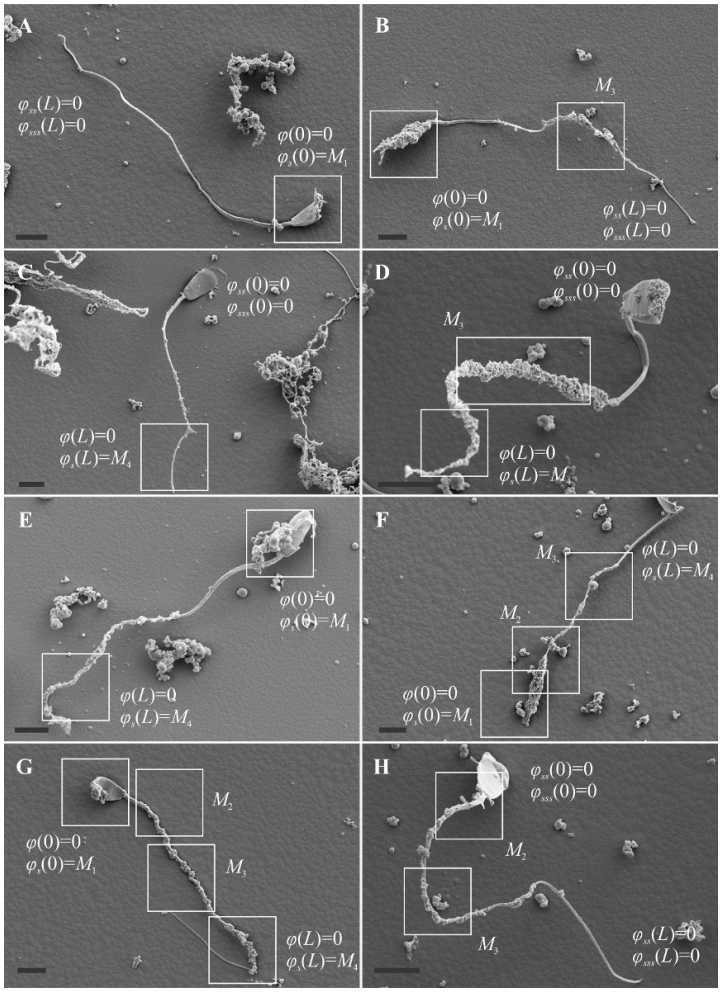

Figure 3.3.
Rice-grain shaped nanoparticles (NPs) adhere to different segments along the sperm cell (The coated segments are indicated with white squares. The scale bar is 5 μm).

Starting from the top-left image and proceeding row by row, we can see firstly an IRONsperm with the head coated with NPs; next, the head and the principal piece are coated with NPs; on the second row, we have two examples where, in the first, the distal end is coated and, in the second, also the principal piece is coated. On the third row, the first picture shows an IRONsperm with head and distal end coated, and the second picture shows a sperm cells with all segments coated except for the head: In the last row, we can see a totally coated IRONsperm and another one with mid-piece and principal-piece coated.

The last image shows only a set of examples of the IRONsperm that we can obtain through this procedure. In fact, since we divided the sperm cell body into four sections and we do not consider the configuration where there is no aggregation between particles and the cell, then the total number of configurations is equal to 15.

In the following table, we are giving an overview of all the configurations. Each group was named using a 4-digits binary code where the most left position is the head and the most right position is the distal end, and the '1' indicates the presence of rice particles:

		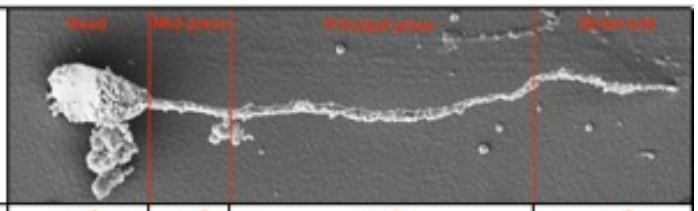			
1	1111	✔	✔	✔	✔
2	1110	✔	✔	✔	
3	1100	✔	✔		
4	1000	✔			
5	0111		✔	✔	✔
6	0011			✔	✔
7	0001				✔
8	1011	✔		✔	✔
9	0101		✔		✔
10	0100		✔		
11	1101	✔	✔		✔
12	1010	✔		✔	
13	0010			✔	
14	1001	✔			✔
15	0110		✔	✔	

To be more precise, we define four magnetic moments m_h, m_m, m_p, and m_d that corresponds respectively to the head, the mid-piece, the principle piece, and the distal end. If the '1' is assigned to a specific section of the body, then, in that section, a magnetic dipole moment is provided to the organic body by the magnetite nanoparticles.
The magnetization profile changes according to the corresponding configuration, in fact, the surface charge of the cell is an important factor in the determination of the magnetization profile of the sperm-templated micro-bio-robot.

Our aim in this work is to deeply study how the flagellar propulsion provided by all the configurations can be influenced by resulting magnetization profile.
The passive flagellum of the cell is considered as an elastic filament surrounded by clusters of nanoparticles and, in fact, the flagellar beat pattern is determined by the location of the nanoparticles along the cell. For example, if the nanoparticles were localized on the head of the cell, a magnetic torque would tend to align the head along the external field lines, and transverse bending waves would initiate and propagate along the passive flagellum.

To fully understand the influence of the nanoparticles on the flagellar propulsion, we can come back to the elastohydrodynamics system based on the regularized Stokeslets theory that we have presented in section 3.1.
The solution to this equation is given by the decomposition of the tangent angle of the flagellum in its zeroth and first Fourier coefficients as follows:

$$\phi(s,t) \approx \phi(s) + \psi(s)e^{j\omega t} + \psi^*(s)e^{-j\omega t}$$

If we assume a cell with four randomly magnetized segments, then the boundary conditions to get the correct solution are selected based on the magnetized segments. For example, if we assume that a sperm cell is magnetized only on the head, then the corresponding boundary conditions will be [14]:

At proximal end:

$$\phi(0,t) = 0 \qquad \frac{\delta\phi}{\delta s}(0,t) = M(0) \tag{3.1}$$

At free distal end:

$$\frac{\delta^2\phi}{\delta s^2}(L,t) = \frac{\delta^3\phi}{\delta s^3}(L,t) = 0$$

If, instead, the magnetite nanoparticles adhere on the head and on the principal piece of the body, then the boundary conditions does not change with respect to previous case, but we have to consider another magnetic moment M_3 applied at the principal piece.

A more in-depth theoretical analysis on the different behaviors of the IRONsperm configurations through the study of the parameters derived by this previous formalization will be presented in the section 6.2. In this latter, we show the waveform analysis and this method leads to conclude that the resultant beat pattern of the hybrid micro-bio-robot is functionally different from that of the active flagellum. This is why it is of interest to consider the attachment of rice particles along the entire cell or along the segments of the cells.
This approach will lead to make theoretical predictions on the motion and on the flagellar propulsion of the micro-bio-robots to be finally compared with experimental results.

Chapter 4

Experimental Setup

The method of actuation needed to control a microagent is strictly correlated to the design of the microrobot: in fact, it is impossible to generate globally optimal designs. According to the type of microrobots we are going to control, we can get different challenges to face and it could lead in the definition of several strategies for the propulsion. For example, the crawling microrobots require more complicated propulsion mechanisms than those for swimming.

In particular, in our field of research we strictly focus on the difference between actuating a motile sperm cell and a immotile sperm cell: except for the method used to control these microagents, the main difference between these two cases is that when you have to deal with motile sperm cells you can control only the direction of the motion and you can adopt the natural propulsion as actuation method. In the second case, the sperm cell is not able to move, and then it is necessary to find an approach that allows to control both the actuation and the direction.

IRONsperm are dead sperm cells coated with nanoparticles: since we are designing a new generation of microrobots that uses as biological part immotile microorganisms, then we need to define a proper actuation method that allows to control the motion of the robot in any direction.
In section 2.3, we have introduced the concept of wireless magnetic actuation describing some of the main features of this control system and some case of applications in the state-of-the-art. In fact, we have illustrated how external magnetic fields can be manipulated in order to develop methods of propulsion that would be impossible for natural autonomous microorganisms.
It has been shown that the sperm motility can be reduced if the cells are prolongedly exposed or exposed to high magnetic field strengths. It is also known that the cells cannot be harmed by a short exposure to low magnetic field, but since our work is based on the utilization of immotile sperm cells, there is no reason to be worried about the status of the sperm cells under the effect of the applied magnetic field. In fact, in the literature, a variety of research groups have proposed several magnetically-driven mechanisms to realize microrobots able to swim at low Reynolds numbers regime.

In this section, we are going to present the experimental setup, with all its main characteristics, that we used to test the IRONsperm and to get the experimental results used for the analysis of the characterization of the frequency response, which will be presented in the next sections of this work. Firstly, we are going to present the actuation method developed for the 5-DOF electromagnetic system for wireless manipulation called "OctoMag". This device offers the chance to understand how the magnetic actuation works, and it was used as a source of inspiration to build our setup.

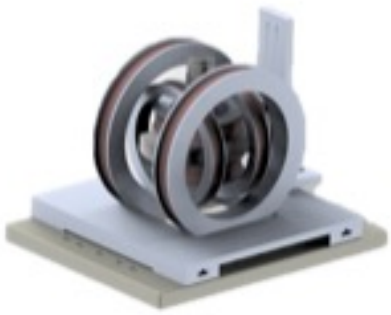

Figure 4.1. Helmholtz electromagnetic system.

This latter, it is called the "Helmholtz setup" and it is the electromagnetic system used to control IRONsperm at the Surgical Robotics Laboratory at University of Twente. The external magnetic torque exerted on the nanoparticles allow us to devise a control strategy that results in a sperm-like motion of the flexible microrobots.
All the components and characteristics of this setup will be introduced in a way that it will be possible to fully understand the different phases of the experimental analysis.

4.1 Octomag Inspiration

Now that we have demonstrated that magnetic fields can be introduced to mimic swimming methods of microorganisms without using onboard actuation systems, we can start presenting the strategies that are of interest for our work.
If we want to control the motion of flexible microswimmers, we need to define a method that allows their remote actuation by the application of an external magnetic field.

With the goal of achieving less invasive and safer retinal surgery, even though it resulted to have potential uses in many other medical applications, M.P. Kummer et al. in [14] designed an electromagnetic system called "OctoMag". The design of this device allows to enable five-degree-of-freedom wireless magnetic control of a fully untethered microrobot: in fact, three degrees of freedom are dedicated to the position control and the left two degrees of freedom manage the orientation control.

OctoMag does not correspond to the system we used for the experimental analysis, but it represents an important inspiration in the literature for the design of a new setup like the one that we will present in the next section. It means that, in this context, we are not interested in the applications and in the results obtained by the OctoMag, but we would like to give an overview of the theory behind the magnetic actuation and the design choices that characterize this system.

The main challenge of this system is to perform 5-DOF wireless control of microrobot in a stationary world frame of reference. As in our case, we assume to control a microrobot with a soft-magnetic body: since the magnetic moment is dependent on the applied field, then it can rotate with respect to the body, and its magnitude can assume large variations in the applied field.

The torque (N/m) on the electromagnet mounted in the setup is expressed as:

$$T = M \times B$$

where B is the value of the flux density of the applied magnetic field at the location of the magnetic moment M. The torque T tends to align magnetic moment M with the flux density of the applied magnetic field B.

The torque T tends to align magnetic moment M with the flux density of the applied magnetic field B. When we consider soft-magnetic bodies, the torque tends to align the longest axis of the body with the field, as in the IRONsperm case shown in figure 4.2, where the longest axis is represented by $e_1(t)$.

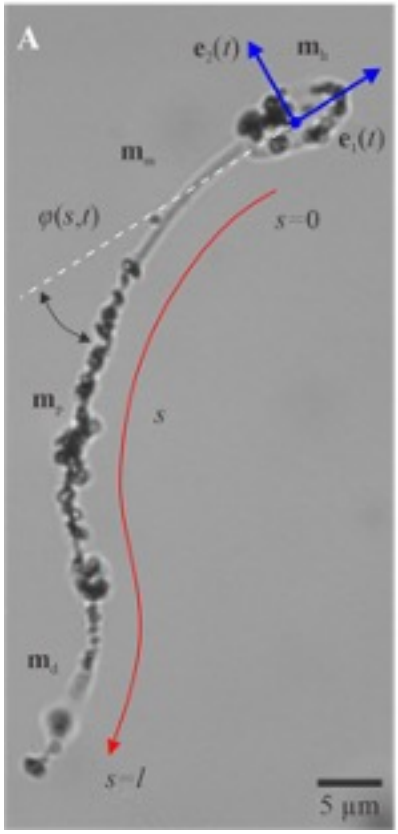

Figure 4.2. IRONsperm formalization.

Assuming uniform magnetization throughout a body it is not possible to control the torque along the axis of M using the model that we just presented. In soft-magnetic bodies, it would involve in the impossibility of performing rotations about the long axis of the body. At this point it is evident that we have to introduce other methods to control the magnetic torque.

The torque on the electromagnet can also be expressed as:

$$T = M \times B = Sk(M)B$$

The force of the magnetic moment is expressed in Newton and can be formulated as:

$$F = (M \cdot \nabla)B$$

But since the region occupied by the body does not present any current flows, then we have from Maxwell's equations the notable result $\nabla \times B = 0$, and, indeed:

$$F = \begin{bmatrix} \frac{\delta B}{\delta x} & \frac{\delta B}{\delta y} & \frac{\delta B}{\delta z} \end{bmatrix}^T M$$

If we consider a workspace point P, then the magnetic field generated by the activation of an electromagnet is expressed as $B_e(P)$, and its magnitude varies linearly with the current through the electromagnet.

For this reason, we can assume an equivalent formalization that describes the multiplication between a unit-current vector (T/A) and a scalar current value (A):

$$B_e(P) = \tilde{B}_e(P) i_e$$

where the e represents the contribution of the e-th electromagnet. Then the magnetic field at a point in the workspace is given by:

$$B_e(P) = \sum_{e=1}^{n} B_e(P) = \sum_{e=1}^{n} \tilde{B}_e(P) i_e$$

Assuming all the definitions enunciated up to now, it is possible to define the desired magnetic torque and force acting on the microrobot as follows:

$$\begin{bmatrix} T \\ F \end{bmatrix} = \begin{bmatrix} Sk(M)B(P) \\ M^T B_x(P) \\ M^T B_y(P) \\ M^T B_z(P) \end{bmatrix} \begin{bmatrix} i_1 \\ \vdots \\ i_n \end{bmatrix} = A_{T,F}(M,P) I$$

where n is the unspecified number of coils. $A_{T,F}(M,P)$ represents the $6 \times n$ actuation matrix and, assuming the knowledge of the microrobot's pose and the magnetic moment, we can finally obtain the current to derive the desired torque/force vector:

$$I = A_{T,F}(M,P)^{+} \begin{bmatrix} T_{des} \\ F_{des} \end{bmatrix}$$

Now that we have explained the theoretical background behind the wireless magnetic manipulation adopted the OctoMag electromagnetic system, we can move on by introducing some design features that characterized this system, and valid also for the next developed setups.

The most important aspect is about the design of the configuration of the electromagnets in the workspace. Using n stationary electromagnets, the most reasonable way to proceed would be to characterize the system with a condition number based on the singular values that define the actuation matrix, since they provide information's on the condition of the workspace, such as points, configurations and where the system results in a loss of control. Unluckily this procedure appears to be too ambiguous and difficult and it is necessary to find another approach. The solution would be to introduce a modified actuation matrix where the field equations can be attenuated, and we have direct control on the force instead of the magnetic torque. Using the force generation capability as reference parameter it is possible to find electromagnet configuration, as shown in figure 4.3 , to achieve the desired performance goals.

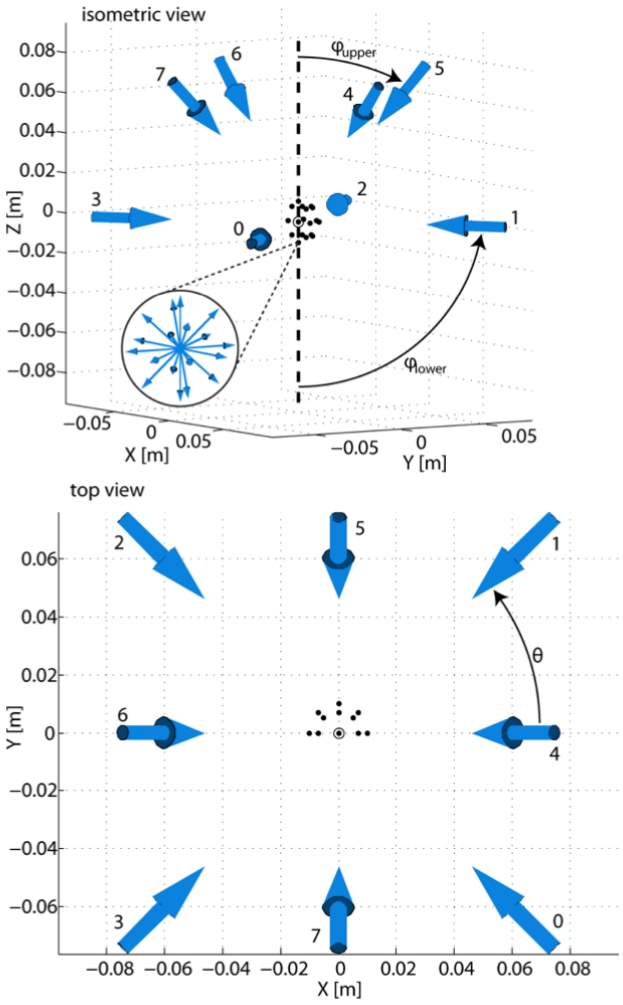

Figure 4.3. Optimization of the OctoMag electromagnet configuration.

In the case of the "Helmholtz" setup, we are not going to apply this design procedure for two main reasons: we are not interested in controlling directly the magnetic field, buut we want to control the magnetic torque; our setup has a more limited workspace and a different kind of coils that allows to avoid the above mentioned problems.
Despite these differences, thanks to the OctoMag system presentation we introduced the main peculiarities that characterize the "Helmholtz" setup too and, in the next section, we will start to give an overview to all its characteristics.

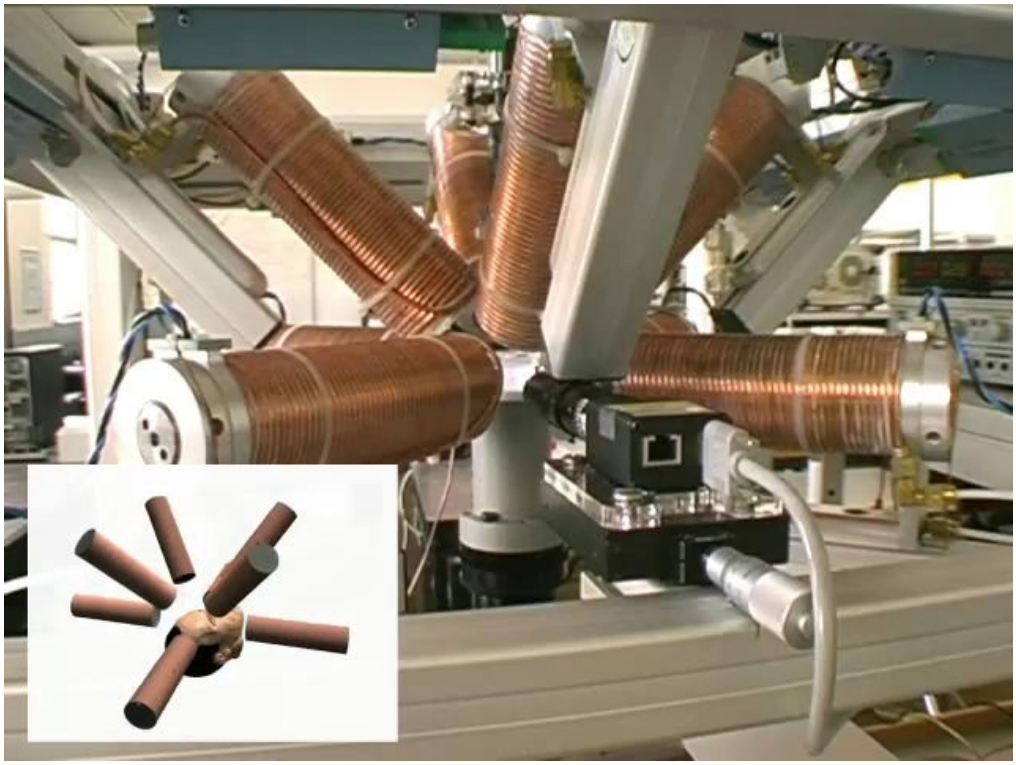

Figure 4.4. OctoMag setup

4.2 Helmholtz Setup

In the previous section, we have presented the characteristics of the "OctoMag" electromagnetic system. We have shown how this system is able to provide wireless magnetic actuation control and how this can be adopted in different fields, especially in the medical field.

In this section, we present the electromagnetic system that we used to actuate our IRONsperm robots and collect experimental data. It was built and installed at the Surgical Robotics Laboratory of University of Twente. We are going to describe its electromagnetic features and all the components that characterize this system.

Below we show the list of all the elements that characterize this system and that we are going to describe in detail:

- Helmholtz coils (6 coils, 3 pairs).
- Motor drivers for current control.
- Microscope for direct visualization of the robots.
- Monocular camera for camera feedback.
- Additional ultrasound probe for ultrasound feedback.
- Computer interface to manage the system.

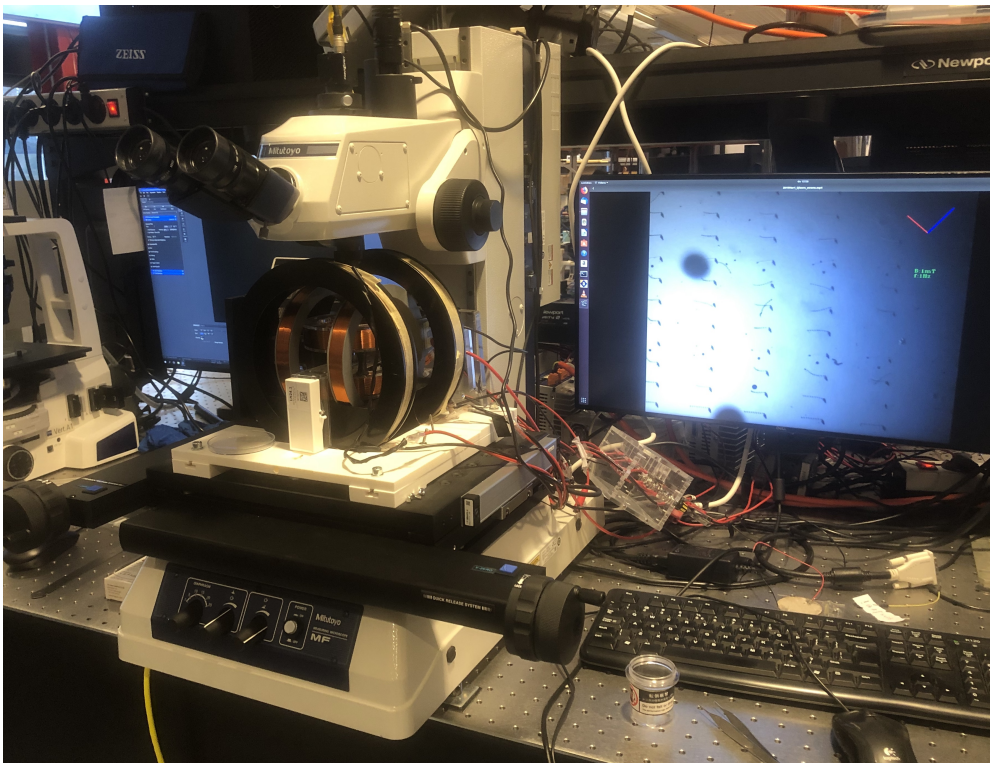

Figure 4.5. Helmholtz Experimental Setup

4.2.1 Helmholtz Coils

This experimental setup was built with the aim to be able to control the motion of different microrobots applying a uniform magnetic field in the region where the micro agents are collocated.
In fact, this system was not built specifically for the IRONsperm experimental phase, but it was used and tested in several occasions with other kinds of micro-bio-robots.

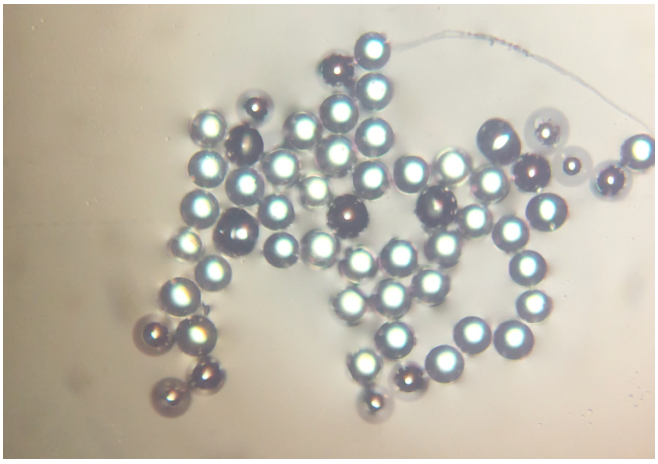

Figure 4.6. Janus Particles in the Helmholtz Experimental Setup

The main difference with respect to the "OctoMag" system is that we used another kind of coils, since we needed to generate a uniform electromagnetic field in a certain region in order to have uniform actuation of the microrobot in any point of the space.

In order to obtain this result, the coils used to produce this magnetic field are the "Helmholtz coils": these devices ,named after the German physicist Hermann von Helmholtz, comprises a set of two electromagnets on the same axis, as shown in the following figure.

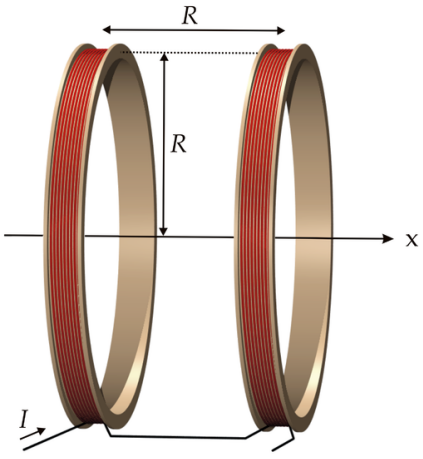

Figure 4.7. Helmholtz coil schematic drawing.

This system is able to produce a region of nearly uniform magnetic field, exactly as needed for our work.

Formally, a Helmholtz pair consists of two circular magnetic coils with the same magnetic characteristics and dimensions, in fact both coils carry an equal electric current in the same direction, and they are both characterized by the same radius R. These are placed symmetrically along a common axis, on two opponents sides of the experimental area, separated by an assigned distance h, which is equal to the radius size R of the coils. The equation $h = R$ is what defines a Helmholtz pair.

Computing exactly the magnetic field at any point in the space is mathematically complex, also due to the involvement of the study of the Bessel functions. If, instead, we consider only the axis of the coil-pair, things get much simpler, and we can assume the Taylor series expansion of the field strength as a function of the distance from the central point of the coil-pair along the axis.
By simmetry, it comes out that the odd-order terms in the Taylor expansion are zero and, if we arrange the system of coils such that the origin, defined as $x = 0$, is identified as an inflection point for the field strength due to each coil separately, then one single coil is able to guarantee that the order term x^2 is also equal to zero. Hence, the leading non-constant term is of order x^4 (it means that the first non-zero derivative is $\frac{\delta^4 B}{\delta x^4}$). This result leads to the following conclusion: the definition of a Helmoltz pair, $h = R$, minimizes the non-uniformity of the magnetic field at the center of the coils. It means that $\frac{\delta^2 B}{\delta x^2} = 0$ is set and a 7% variation in the field strength is left between the center and the planes of the coils. Generally, the inflection point is located along the coil axes at a distance $R/2$ from its center, and, hence, the location of the two coils are $x = \pm R/2$.

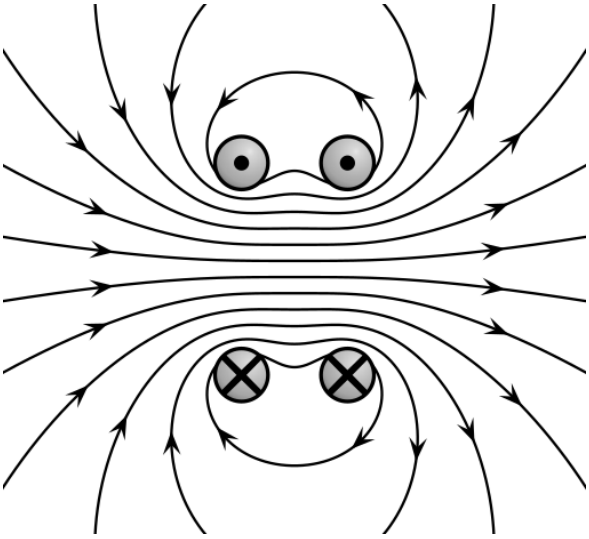

Figure 4.8. Magnetic field lines in a plane bisecting the current loops

To derive the value of the generated magnetic field, we have to start from the on-axis field due to a single wire loop formula, which is derived from the Biot-Savart law and it is defined as:

$$B_1(x) = \frac{\mu_0 I R^2}{2(R^2 + x^2)^{\frac{3}{2}}}$$

Where:

- μ_0 is the permeability constant $4\pi \times 10^{-7}\ Tm/A = 1.257 \times 10^{-6}\ Tm/A$.
- I is the coil current in Amperes.
- R is the coil radius in meters.
- x is the coil distance, on axis, to point, in meters.

A parameter that characterizes a Helmholtz coil is the number of turns of wire n. From this, we can deduce that the current that flows in a one-turn coil is $1/n$ times the current I that flows in a n-turns coil. Then we can arrange the previous equation for a n-turns coil:

$$B_n(x) = \frac{\mu_0 n I R^2}{2(R^2 + x^2)^{\frac{3}{2}}}$$

If we compute the magnetic field strength in the halfway point between the coils $x = R/2$, we get:

$$B_n\left(\frac{R}{2}\right) = \frac{\mu_0 n I R^2}{2(R^2 + \left(\frac{R}{2}\right)^2)^{\frac{3}{2}}}$$

Since we have two coils, one at $x = 0$ and one at $x = R$, for symmetry, we can obtain the final measure of the magnetic field strength at the midpoint by multiplying by 2:

$$\begin{aligned} B\left(\frac{R}{2}\right) = 2B_n\left(\frac{R}{2}\right) &= \frac{2\mu_0 n I R^2}{2\left(R^2 + \left(\frac{R}{2}\right)^2\right)^{\frac{3}{2}}} \\ &= \frac{2\mu_0 n I R^2}{2\left(R^2 + \frac{R^2}{4}\right)^{\frac{3}{2}}} = \frac{\mu_0 n I R^2}{\left(\frac{5R^2}{4}\right)^{\frac{3}{2}}} \\ &= \left(\frac{4}{5}\right)^{\frac{2}{3}} \frac{\mu_0 n I}{R} = \left(\frac{8}{5\sqrt{5}}\right) \frac{\mu_0 n I}{R} \end{aligned}$$

Thanks to these devices, we can build up a setup like the one shown in the following figure.

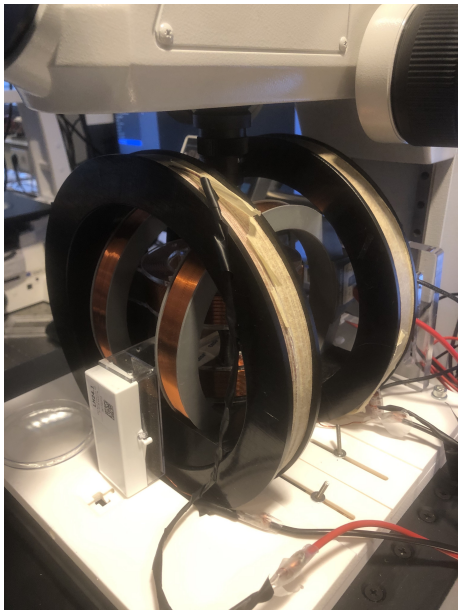

Figure 4.9.
Helmholtz coils in the experimental setup at Surgical Robotics Laboratory (University of Twente).

As just mentioned, the use of 6 coils is primarily to get a uniform magnetic field along all the directions. The main benefit of this characteristic of the system relies on the actuation of the IRONsperm during the experimental phase: in fact, if the system of coils properly works, it possible to control the motion of the IRONsperm along any direction in the experimental area. As we will see in detail in section 5.1, to control the swimming motion of the micro-bio-robot in the fluid it is necessary to have control on the z-axis motion. The swimmers are subject to the force of gravity during the motion and, if they fall down to the lowest layer of water then they will be influenced by different boundary conditions and the experiment will be invalidated. Thus, controlling the motion along the z-axis allows to manage this phenomenon as much as needed to conduct properly the experiments.

In any electromagnetic system, we need to develop and use coil driver to make the system works as desired. In fact, the coils are used in magnetic manipulation system by adjusting the amplitude of the current [14]. The most frequently used technique for controlling the current is the Pulsewidth modulation that provides high, efficiency, low power loss, and robustness to noise.
When we use this method at low frequencies, as in our case, then PWM produces high-magnitude current ripples, and it results in magnetic field fluctuation that limits the operating time of the coils and decreases the predictability of the magnetic field, that is essential for wireless magnetic manipulation.

For our system, coil drivers have been developed specially to minimize the magnetic field fluctuations and, as a consequence, they are able to improve the motion resolution of magnetic manipulation systems. Moreover, magnetic manipulation and drug

release can be performed using the developed driver without an external magnetic induction unit, which decreases the complexity of the system [9]. These drivers were test using air core coils, iron core coils and, finally, Helmholtz coils, monitoring the current through the coil terminals, the magnetic field magnitude, and the ohmic loss while the PWM frequency is varied.

4.2.2 Feedback Systems and Computer Interface

The coils and the motor drivers that control the current flow are the elements that compose the electromagnetic system of the experimental setup used to analyze the motion of the IRONsperm. Additional elements, as the feedback systems and the panel control, complete the experimental setup.

We use an electromagnetic system to provides uniform weak magnetic fields to move and steer IRONsperm in a three-dimensional space. Simultaneously, during the characterization of the frequency response of the IRONsperm configurations we use imaging system composed simply by two elements: the microscopy and the linked camera.

Position of the micro-bio-robots is detected using a microscopic system. The microscopy mounted in this setup is the Mitutoyo MF Series 176 Measuring Microscopes, and using a 10x Mitutoyo phase objective it is possible to visualize and check the excitation of the swimmers under the influence of the external magnetic field, and keep track of the robots inside the fluid during the control of the motion in real-time. Moreover we linked a avA1000-120kc Basler Area Scan Camera to the microscopic system such that we can transmit a magnified image of what we see under the objective of the microscope. In fact, the camera is linked to the computer and the image is shown on the computer interface that we are going to describe in this section.

The camera system used to localize the IRONsperm during the characterization of the frequency response is a good and useful feedback system only during the in vitro experimental phase.
Imaging of micro-robot system is one of the big difficulties for many in vivo micromotor applications. In fact, an efficient three-dimensional, non-invasive, deep-tissue, and high-resolution imaging system is still a challenge to be demonstrated. Different imaging techniques have been tested such as optical fluorescence, infrared emission, X-Ray analysis or Ultrasound Imaging. More recently, a new area that couples ,via the photoacoustic effect, light excitation to acoustic detection called “Photoacoustic imaging” .

Another important strategy to make the micro hybrid structures visible through the human body could be the use of high-resolution ultrasound detectors.
This is the additional imaging system that we already tested for our micro-bio-robots since, in the latest years, it was demonstrated that ultrasound can be used to image microparticles. In fact, Ultrasound is able to penetrate into deep tissue without harm neither for the body (it is used in medical examinations to image organs and tissues) nor for the sperm cells. In the field of the imaging systems for this kind of application, only ultrasound can combine good resolution, minimal adverse health effects, high speed, safety and adequate frame rates.

In the following image, we can see the ultrasound visualization of the IRONsperm in the experimental setup. The figure demonstrates that it is possible to detect the IRONsperm using ultrasound imaging. Anyway, this method must still be studied

in-depth to get a high-resolution localization with no ambiguities.

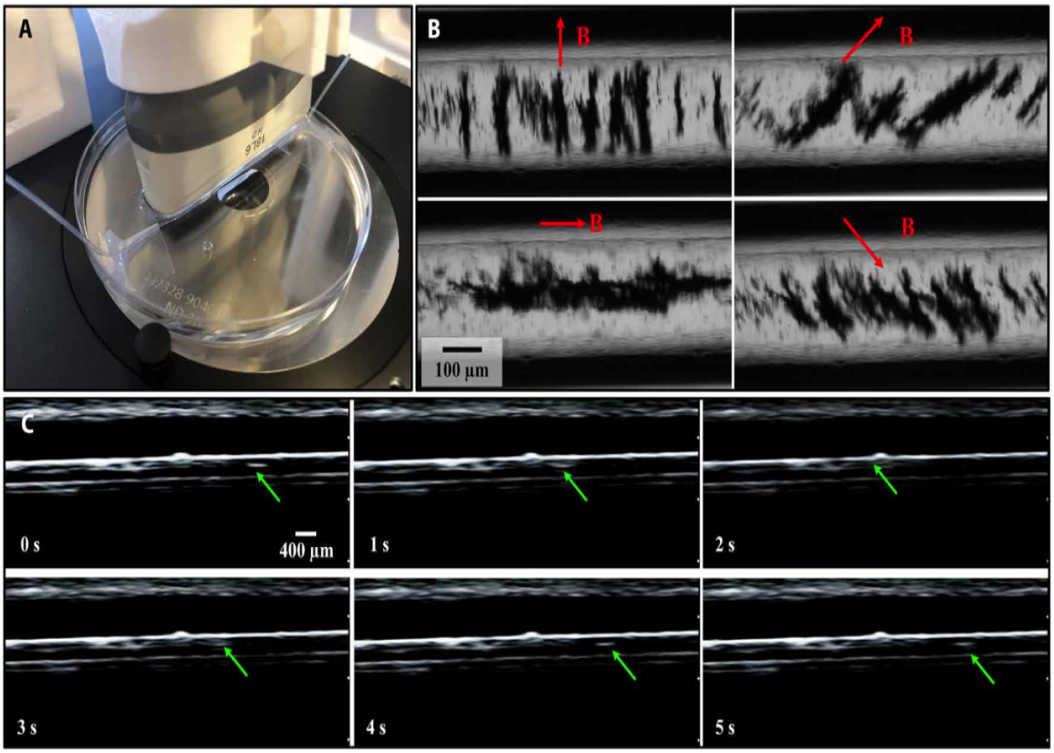

Figure 4.10.
Ultrasound images showing efficient localization of a cluster of IRONSperm. (A) Clusters of IRONSperm samples are contained inside a polyethylene tube with an inner diameter of 380 μm. (B) Visual feedback is obtained by the microscopic images and indicates several clusters that align with the external magnetic field lines (red arrow). (C) Ultrasound scans show a cluster of IRONSperm samples (green arrow) moving with the flowing streams of the medium along one dimension [19].

As the camera visualization, also the ultrasound imaging is transmitted to the computer interface.
This latter is the last component of the experimental setup that we are going to describe. It is the connection point between the two groups of elements that we have presented in this chapter. In fact, thanks to this interactive interface it is possible to keep track of the position of the IRONsperm in real-time and, simultaneously, to control the magnetic field all the parameters that affects its shape.

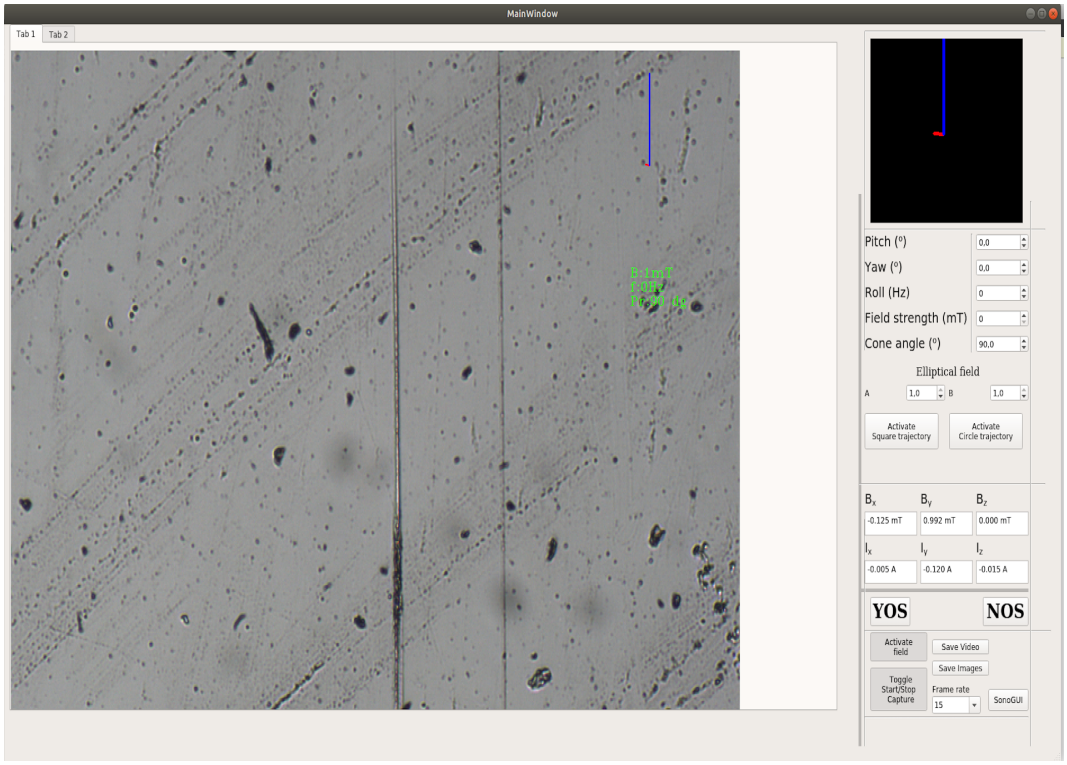

Figure 4.11.
User Interface to control the Helmholtz setup during the experimental analysis.

The above image shows how the computer interface works during an experiment that uses the camera imaging system: on the left, it is shown the visualization of the microrobots in the setup that can be registered; on the right, there a commands column that allows to define the Roll, Pitch and Yaw angles of the magnetic field, the cone angle of the field (always set to 90° during the experimental phase of this work), the intensity of the magnetic field in mT. It shows also the current values of the current components transmitted to the system, in order to avoid overloading the system. Finally, it is also possible to display the trajectory to be tracked during the trajectory steering experiments that we are going to mention in the next chapter.

Chapter 5

Motion Analysis

In the previous sections, we have reported the specifications of the system that we used during this project and we provided a detailed description of the microagents that we want to test and analyze.

The particular interest of this work is to evaluate the motion behavior of these micro-bio-robots in a fluid characterized by a low Reynolds number. As we have explained, thanks to wireless magnetic manipulation we are able control both the propulsion and the direction of the IRONsperm. The application of the external periodic magnetic field produces a motion of the magnetized sperm cells and the correct management of the parameters of the field allows to drive and steer these devices.
The major goal of this work is to investigate on how the magnetization profile influences the flagellar propulsion of IRONsperm. In order to achieve this aim, we need to analyze the motion behavior of all the fifteen configurations of the robot.

In this section, we are presenting the characteristics of the different phases of analysis that we conducted during this work. We will describe the procedures that we defined in order to analyze the motion of the IRONsperm under different perspectives. In fact, three different kinds of analysis are going to be presented: the characterization of the frequency response; the waveform analysis; and the trajectory steering control. The first allows to analyze the motion behavior of all the configurations of these devices within a given range of frequencies. The second, capturing different wave cycles of the motion of the flagellar propulsion of the IRONsperm, extracts the parameters that defines the waveform of the robot and it produces the expected velocity. The third corresponds to a practical test where we tried to drive and steer different configurations of these micro-bio-robots for open-loop guidance along a treajectory. This latter gives the chance to make important considerations on the control features that characterize this robot, but it is not object of result analysis in this work since it is still in a premature phase. The first and the third propose and experimental point of view to introduce the motion of the IRONsperm and its features during a real application. Contrarily, the waveform analysis is a theoretical approach to define the characteristics of the flagellar propulsion.

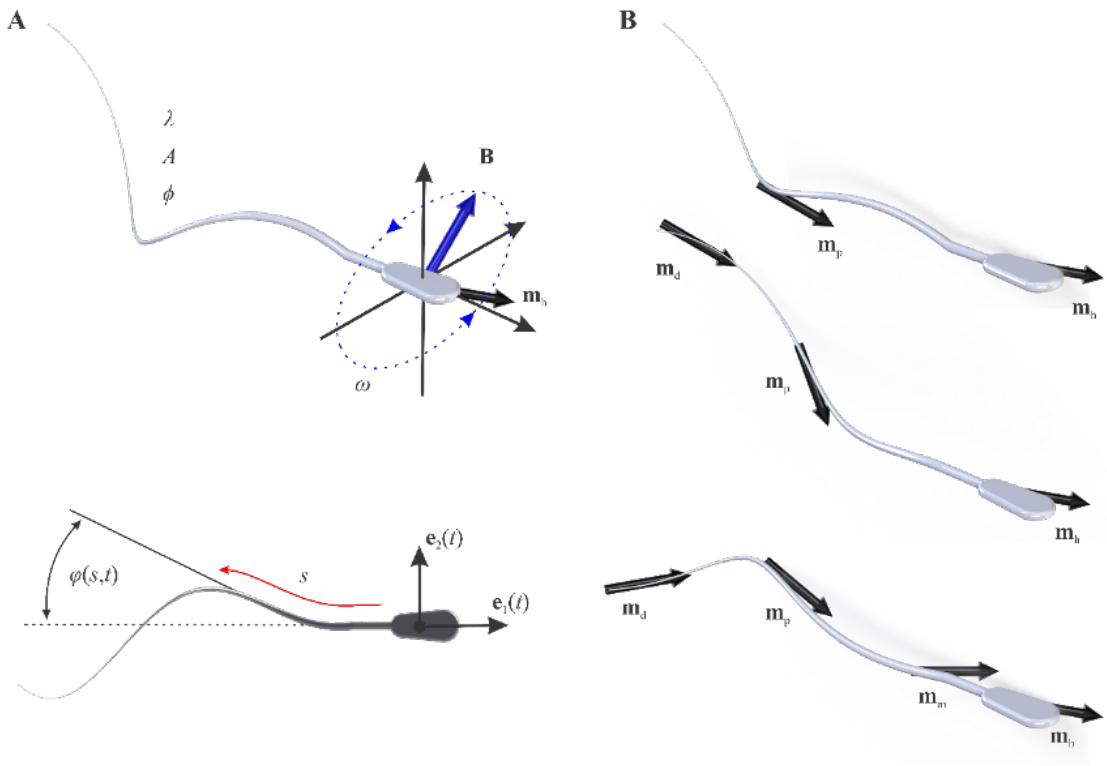

Figure 5.1.
Flagellar waveform of the micro-bio-robots is influenced by the magnetization profile along the flagellum. (A) Rotating magnetic field (B) exerts magnetic torque on the magnetic head, at angular frequency (ω). The induced bend results in a travelling wave along the flagellum characterized by the angle ($\phi(s,t)$ between $e_1(t)$ and the local tangent along s. (B) The flagellar beat pattern depends on the magnetization of the mid-piece (m_m), principal piece (m_p), and distal end (m_d).

The combinations of these results will be analyzed in the next sections, and finally it will be provided a comparison to give our conclusions on the analysis proposed in this work. In the next paragraphs, we are giving an overview of the different kind of analysis in order to allow the reader to understand the final presentation of the results.

5.1 Characterization of the Frequency Response

In this work, we show the influence of distributed bending moment and localized external actuation obtained through the application of positively charged ferromagnetic nanoparticles on the flagellum of bull dead sperm cells. The first step to do in order to have a better comprehension of the motion features of the robot is to have a direct observation on its behavior under stimuli at different freuqencies.

The incorporation of new nanoparticles opens up additional possibilities since these particles will selectively adhere to certain locations along the flagellum, and it will involve in enabling non-uniform distributed magnetic actuation. One method to investigate the influence of the charge distribution of the micro-bio-robots involves actuation by a periodic magnetic torque. The dynamic response to this periodic torque can efficiently be used to distinguish between the groups of hybrid micro-bio-robots. In fact, the ferromagnetic particles that coat the body of the sperm cells provide a dipole moment and allows to the flexible flagellum to align along the oscillating weak magnetic field lines. It generates a propulsion thrust force that overcomes the drag force and produce a motion that we want to inspect.

Our inspection in the motion features of the different configurations of the IRONsperm will proceed with the characterization of the frequency response of a set of samples for each of these configurations. This characterization of the frequency response will be evaluated in the frequency range that goes from 0 to 20 Hz and it allows to derive and discuss the properties and the features that characterize the fifteen groups of micro-bio-robots. The choice of the selected frequency range is based on previous experimental phase and analysis of the literature that suggest that the dead sperm cells behavior is not significant out of that range.

The electromagnetic configuration used this experimental analysis is the Helmholtz setup that we have presented in section 4.2. The three pairs of coils apply an oscillating weak magnetic field with a magnitude equal to 3 mT. This magnetic coils configuration is used to provide the periodic magnetic field and achieve flagellar propulsion in 3D space. In fact, the use of 6 coils leads to get a uniform magnetic field along all the directions. The main benefit of this characteristic of the system relies on the actuation of the IRONsperm during the experimental phase: in fact, if the electromagnetic system provided by the set of coils properly works, it is possible to control the motion of the IRONsperm along any direction in the experimental area and it implies that the IRONsperm can dive and swim with a uniform propulsion in any direction.

The actuation of the IRONsperm does not depend only on the kind of configuration the hybrid device belongs to, but also some external agent can affect the actuation. The most relevant is surely the water flow that moves the sperm cells inside the analyzed sample. Generally, it is simply caused by the incline of some degrees of the slide where the sample is on, but when the frequency is increased, this water flow becomes more problematic since it starts to move clusters inside the sample, and it can invalidate the motion analysis of the IRONsperm. Moreover, as mentioned in section 3.2, the swimming control of the micro-bio-robot in

the fluid is not trivial and it is necessary to have control on the z-axis motion. Due to the force of gravity, the swimmers fall down to the lowest layer of water during the motion. If it happens their motion behavior can be obstructed by cluster of sperm cells and invalidated due to the influence of different contours conditions.

The correct setting of the experimental setup is fundamental for the investigation of the motion behavior of the IRONsperm. During the experimental phase, not all the micro-bio-robot are good to analyze and this is why we have to find what we call the "good swimmer": a good swimmer is a sample that is able to present, at the same time, balance between elasticity of the tail, that is very important also for the waveform analysis since it allows to capture the flagellum deformation over the beat cycle, to provide propulsion, since it is the results of the non-uniform actuation of the magnetic field and it characterizes the different configurations of this device, and, finally, the magnetic response, that confirms the correct behavior of the control system since the IRONsperm aligns with the magnetic field direction.

Another relevant aspect to highlight is the swimming direction of the micro-bio-robots: in fact, due to different particles distributions that implies a different magnetic response, it is possible to see how the IRONsperm samples swims either in the forward direction or in the backward direction. This is not necessarily a problem, but we wanted to investigate on this feature in order to find out why it happens and if it influences the performances of our devices. During the experimental phase, we gave important attention to this phenomenon and we wondered how we can modify these behaviors in order to get an IRONsperm that moves always in the same direction (forward or backward). The only method that does not interfere with the experimental procedure was examined and it corresponds to a simple rotation of 180° of the magnetic field direction in order to invert also the swimming direction of the IRONsperm.
It came out that this approach con produce three different effects. These are the following:

1. The first one is the ideal case, where the swimmer changes direction without rotating and it starts to move as desired.

2. The second one is when the swimmer starts to rotate such that he can follow the magnetic field direction without modifying its behavior. It implies no changes in the swimming behavior of the IRONsperm and the problem is not solved.

3. In the third case, the swimmer starts to deform and it is very dangerous since it may lead to invalidate the swimmer actuation.

It is still not possible to conclude what are the conditions that produce these different effects. Since this work is concentrated on the motion analysis of the IRONsperm and not on its control features, we decided to take note of this behavior and to address it to a future evaluation. The third case explains that this approach can be dangerous since it would invalidate a good swimmer instead of getting a desired better performance and it would imply the reduction of the chances to get consistent

results for the motion analysis in an acceptable time.

Once that all the important aspects of this analysis are assumed, we can proceed with the experimental phase and produce all the results that characterize our micro-bio-robot. It is important to highlight the fact that the configurations that we have defined are just an approximation of the real distributions of magnetic nanoparticles along the body of the sperm cell. In fact, the motion of the two IRONsperm cells belonging to the same configuration can differ because the motion of these devices is strongly influenced by the location of the adhesion of the nanoparticles. Since the length of the sperm cells is about 70 μm then it is easy to understand that the distribution of particles can be very different even between two samples belonging to the same configuration. In order to solve this problem, the most immediate solution was to collect enough data for each configuration in order to get a consistent trend. This problem will be discussed in detail in the section 6.1.

The frequency response of the IRONsperm under the actuation of external periodic magnetic field lines can be used to efficiently control its swimming speed during different kinds of control tasks. In fact, the field is used for both actuation and directional control and the characterization of the frequency response allows a comprehension of the properties of the micro-devices with respect to the magnetic moment distribution and the frequency of the weak magnetic field.

5.2 Waveform Analysis

In the previous section, we presented how to proceed with the experimental analysis in order to investigate on the influence of the magnetization profile on the flagellar propulsion of IRONsperm. This type of analysis allows to extract data from the actual motion behavior of all the configurations of the micro-bio-robots under the actuation of an oscillating weak magnetic field that exerts a magnetic torque on the positively charged nanoparticles applied on the sperm cell body.

The characterization of the frequency response analysis can be interpreted as a first approach to the inspection of the motion characteristics of these new devices. In fact, the process that characterizes this analysis is trivial and basing all our investigation only on that approach would make the whole analysis too poor. This is the reason why we decided to view the motion behavior of the IRONsperm from an additional point of view: we conducted a different analysis that allows to make theoretical predictions on the behavior of each configuration of IRONsperm. This is called waveform analysis and, as suggests the name, it exploits the characteristics of the waveform pattern while the sample is swimming. This pattern can be translated into three parameters, that are the mean flagellar curvature, the amplitude of the bending moment and the wavelength of the principal flagellar bending wave. Thanks to the combination of these parameters with the Resistive Force Theory defined by Gray and Hancock, it is possible to predict the propulsive thrust of the IRONsperm.

This analysis is based on the work published by Friedrich et al. in [6] where they characterized the waveform pattern of a bull sperm cell using the above mentioned approach. It represents a strong starting point of our investigation and, in fact, an important work was already published in [13] by Khalil et al. where one configuration of the IRONsperm is compared to the same sperm cell waveform model computed by Fredrich et al..

This project is addressed to complete the motion analysis of all the configurations of the IRONsperm and extract the most important conclusions from this investigation. In this section, we describe in detail the waveform analysis that allows to investigate the dynamic behavior of the groups of hybrid micro-bio-robot with various magnetization profiles based on the spatial configuration of the nanoparticles aggregates with respect to the head, the mid-piece, the principal piece and the distal end of the cell, since the magnetization profile of the groups results in a unique waveform during travelling wave propulsion. Finally, in the next and final chapter of this work, we are going to present the results obtained using this approach and compare them with the performances obtained during the experimental phase.

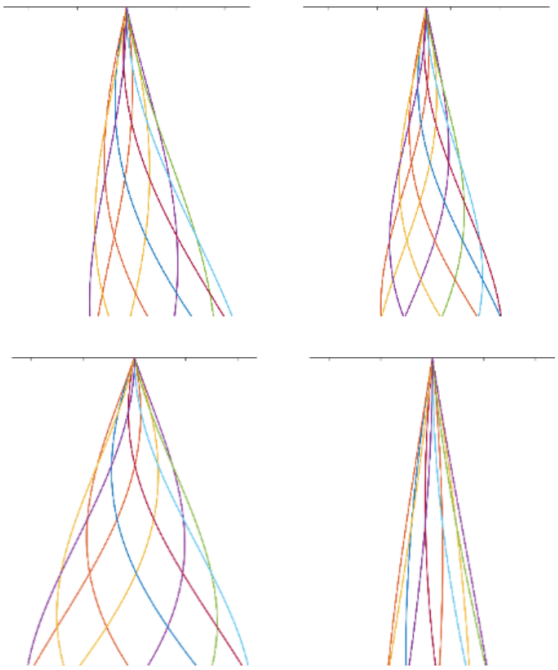

Figure 5.2. Different examples of swimming wave patterns.

This method implies to simulate the propulsion of the IRONsperm using a numerical model that results in the characterization of the flagellar waveform that can be used to distinguish between the groups of hybrid micro-bio-robots.

The movement of any length of the tail of a sperm cell can be described in terms of form and speed of the propagation of the bending waves which travel along the tail [8]. It results in the possibility to determine the path along which a sperm cell swims using the shape of the flagellar beat.
As we have shown in section 3.2, the propulsion of a sperm cell relies on a balance between the tangential force acting along the body and the propulsive forces acting normally on the surface of the body. In fact, any region of the body eliciting from the water a reaction normal to its surface must have a component of motion normal to this surface [7] and it results in balancing between forces and torques generated by the beating flagellum.

The fine structure of IRONsperm is characterized by the tangent angle $\phi(s,t)$ enclosed between, as shown in the next figure, the long axis $e_1(t)$ of the head and the local tangent along the arc length s. According to [8], the inertial forces are negligible and the relation between the viscous force and the velocity of a segment is linear over the beat cycle of the flagellum.
Therefore, the dynamic model described in section 3.1 that defines the motion of the IRONsperm can be solved applying the boundary conditions that are dictated by the magnetization profile of the robot since they are defined according to the distribution of the magnetic moment along the body of the robot.
Proceeding with the analysis, as we mentioned in section 3.1, the tangent angle of

the flagellum is a solution of the dynamic model and it can be decomposed through Fourier decomposition:

$$\phi(s,t) \approx \phi(s) + \psi(s)e^{\iota\omega t} + \psi(s)^* e^{-\iota\omega t}$$

where the $\phi(s)$ is defined as the zeroth Fourier mode and it indicates the time-averaged mean shape of the flagellum. Whereas, $\psi(s)$ and $\psi(s)^*$ are the first mode and its complex conjugate, whose magnitude describes the bending amplitude along the flagellum. We consider only these two modes since it was proved that the higher modes contribute less than 5% to the power spectrum of the tangent angle at all arc-length positions s.
The dynamic model gives the foloowing relation between the hydrodynamic and magneto-elastic coupling:

$$\frac{-i}{l_\omega^4}\left(\psi e^{\iota\omega t} - \psi^* e^{-\iota\omega t}\right) = \frac{\delta^4\phi}{\delta s^4} + \frac{\delta^4\psi}{\delta s^4}e^{\iota\omega t} + \frac{\delta^4\psi^*}{\delta s^4}e^{-\iota\omega t}$$

where l_ω^4 is the characteristic penetration length and it is equal to $\left(\frac{\kappa}{\omega c_{n_i}}\right)^{1/4}$. It shows that the length and the stiffness of the body are related. This is easily understandable because, in fact, if the body is rigid then we do not get a waveform pattern.

To solve the equation, it is important to highlight the fact that from the zeroth and first Fourier mode it is possible to derive three parameters which characterize key features of the shape of the flagellar beat:

- Mean Flagellar Curvature K_0:
  It is defined by fitting a line $K_0 s$ to the zeroth mode $\phi(s)$. It provides a measure for the asymmetry of the mean shape of the flagellum: ideally, the waveform is symmetric, and the cell moves along a line, whereas, in the real case, the waveform is asymmetric, and the flagellum always tends to swim towards one direction defined by the asymmetry. The ideal case corresponds to $\phi(s) = K_0 s$, an it means that the mean shape of the flagellum is curved in a perfect arc with constant curvature K_0.

- Amplitude of the bending moment A_0:
  It is defined by fitting a line $A_0 s$: to the absolute value of the first mode $|\psi(s)|$. The ideal case occurs when the bending amplitude increases linearly along the flagellum and it is defined as $|\psi(s)| = A_0 s$.

- Wavelength of the principal flagellar bending wave λ:
  It is obtained by fitting the line $2\pi s/\lambda$ to the phase angle $\Phi(s) = -\arg\psi(s)$. The ideal case is when $\Phi(s) = 2\pi s/\lambda$ corresponds to a travelling wave with uniform wavelength λ and wave speed $\lambda\omega/2\pi$.

Assuming that the penetration length is nonzero when the frequency is different from zero, in ideal conditions and considering that

$$\frac{\delta^4 \phi}{\delta s^4} = 0 \tag{5.1}$$
$$\frac{\delta^4 \psi}{\delta s^4} = 0 \tag{5.2}$$
$$\frac{\delta^4 \psi^*}{\delta s^4} = 0 \tag{5.3}$$
$$\tag{5.4}$$

We obtain

$$Re\{\psi(s)\} \sin \omega t + Im\{\psi(s)\} \cos \omega t$$

This equation allows to define the phase angle $\Phi(s) = -\arg \psi(s)$ that characterizes the progression of the wave along the flagellum.

Given this equation it is possible to derive the three parameters that we have defined above:

- Measuring the flagellum deformation can be derived the tangent angle $\phi(s,t)$ and once that it is defined it is possible to obtain the zeroth and first Fourier modes.
- The zeroth Fourier mode $\phi(s)$ is used to determine $K_0 s$ by fitting a line to the data.
- Similarly it is possible to derive the amplitude $A_0 s$ by fitting a line to $|\psi(s)|$.
- Finally, we measure the phase angle and we derive the wavelength λ of the principal flagellar bending wave as explained before.

Once that we have measured the wave variables it is possible to derive the force exerted by the flagellum as indicated by the Resistive Force Theory. The deformation can be used to determine the force, given the tangential and normal component of the drag coefficients, respectively c_{t_i} and c_{n_i}, we get:

$$F = \int_0^\lambda \frac{(c_{n_i} - c_{t_i}) y_t y_x - f\lambda(c_{t_i} + c_{n_i} y_{xx}^2)}{1 + y_{xx}^2} dx$$

where x and y are cartesian coordinates on the plane such that we can define $y_t = \frac{\delta y}{\delta t}$, $y_x = \frac{\delta y}{\delta x}$ and $y_{xx} = \frac{\delta^2 y}{\delta x^2}$.

Once we have the characterization of the wave pattern produced by the flagellum, it is possible to compute the force exerted by the flagellum. Using Regularized Stokeslets method, thanks to thia latter result it would be possible to predict the velocity field due to force f at points r along the flagellum of the sperm cell.

Before of concluding this procedure, we need to highlight some assumptions since the idealities of the theories that we have used differ from the observed facts:

- The movements executed by elements of the tail at the two ends are different from those situated centrally. Then the value for amplitude and wavelength must be computed as an average for the different stokeslets that describes the body of the IRONsperm and over a complete beat cycle.
- The oscillation of the head is neglected during the travelling propulsion. The head oscillates at each beat cycle for a distance similar to its forward displacement, but theoretically the effect of the head on the rate of forward propulsion is small.

The procedure to define the theoretical predictions is over. This kind of analysis is really important in order to compare the experimental results and understand the best features of the motion of the different groups of hybrid micro-bio-robots, but it is not the only reason for which we are pushed to use this approach. In fact, the importance of this method relies also on the fact that the actuation of passive flagella reveals insights into the desirable flagellar waveforms and this information can be used to design efficient microswimmers [13].

5.3 Trajectory Steering Control

Contrarily to the other methods of analysis that we presented and described in the previous sections, now we are going to discuss about an another approach that provides different results and considerations with respect to the conclusions shown in this work. The importance of these achievements will be evaluated in the future phases of the project.

Since in this work we are proceeding with a motion analysis, we want to explore and find out all the main features that contradistinguish this hybrid micro-bio-robot. For this reason, we produce and evaluate the results only from the first two type of analysis. This analysis represents a test bench to inspect the control features of the system to improve the experimental phase and future analysis. This is a manual control approach used to recognize and verify issues that may occur during the experiments.
The trajectory steering control follows the same procedure adopted for the characterization of the frequency response analysis. Once we find a good swimmer in optimal conditions, we can start the experiment: we can choose between two kind of trajectories to follow that correspond to a circle and a square. The goal of the experiment is to drive and steer the micro-bio-robot in order to move along the trajectory as accurately as possible.

Even though it could look like a trivial task, it is not at all. As mentioned in the previous sections, controlling the robot during the characterization of the frequency response was not easy, and we did not have to follow an assigned scheme. Now, it is much more difficult. This approach allowed to discover and reflect on all the external agents that influence the motion behavior of the IRONsperm. In fact, the water flow that interferes with the direction of the hybrid device is totally evident. The easiest way to note this problem is given by the fact that the motion of the swimmer is more fluent in certain directions with respect to others. As this issue, many other came out thanks to this kind of analysis.

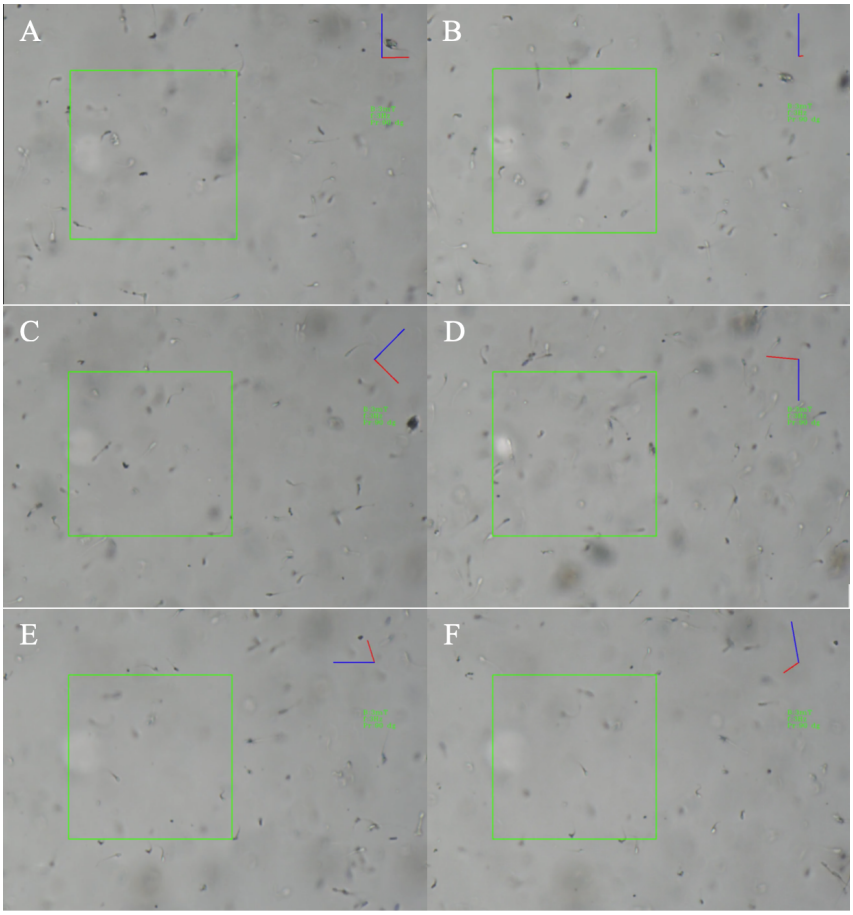

Figure 5.3.
Motion along a trajectory: IRONsperm 0001 is commanded to move along a rectangular trajectory.

This approach is also important to evaluate the response to the magnetic field. In particular, when we use the circle trajectory, we need to keep changing the angle of the magnetic field in order to move along the whole circle. This process highlights the fact that the samples, even if they are considered as "good swimmers", they do not always respond as desired to the magnetic actuation. This is probably caused by the different distribution of nanoparticles on the body of the sperm cell.

By the way, as mentioned at the beginning, this work is not focused on the control features of the IRONsperm. For this reason, the analysis was not conducted on all the configurations and for all the frequencies. It was used only as a basis and a small view for the future developments since these aspects are relevant to be considered for the next phases of the project.

Chapter 6

Results

In the previous chapters, we reported the main features and the aspects that characterize the new micro-bio-robot called "IRONsperm". We introduced and described the characteristics of the experimental setup needed to proceed with the experimental analysis and to extract the data necessary for the motion analysis of this hybrid device.

We have to keep in mind that the final aim of this work is to investigate on the influence of the magnetization profile on the flagellar propulsion of the IRONsperm and to achieve this task we chose to approach the problem following two methods: the characterization of the frequency response in a frequency range that allows to return significant results ; modeling the robot and isimulating the motion using a mathematical model to extract a number of parameters that characterize the waveform propulsion of each configuration. In this chapter, we are going to exploit these two approaches in order to get an in-depth analysis of the behaviour of our robot.

We will describe and comment the results provided by the characterization of the frequency response: here, it will make possible to evaluate which are the configurations that present a good trend, in terms of velocity, over the considered frequency range. These results lead to the first considerations that will suggest what are the profiles to be discarded and the ones to be kept. Implicitly, these conclusions will be very important for the design purposes of the IRONsperm.
The waveform analysis consists in extracting the data from a sufficient number of beat cycles to characterize the wave pattern of the different configurations of the micro-bio-robot. As in the previous analysis, this method will give the opportunity to classify the 15 configurations collecting a set of results that allows to highlight the features of the groups of robots from an alternative point of view.

Finally, the combination and the comparison of the results provided by the two approaches will provide a consistent set of data to make the final conclusions of our work and, indeed, choosing the best features to characterize the final design of our robot to be used in the future phases of the project.

6.1 Experimental Results

This section is dedicated to the description of the experimental procedure and the evaluation of results collected during this phase.
This method led to extract the characterization of the frequency response in the frequency range which goes from 1 to 20 Hz for all the fifteen configurations of the IRONsperm.

We provided all the elements needed to understand the experimental method that we adopted to collect the desired results: in chapter 3.1, we described the main aspects that characterize the design of our robot and the magnetic and the elastic properties that it is expected to provide; in chapter 4.2, we gave instructions on how the experimental setup and the electromagnetic system are used in order to achieve our tasks during these procedures; and, finally, in chapter 5,we introduced the specific details of this approach.
Assuming all this information, we can proceed with the description of this phase and with the analysis of the results.

Before of showing the main results of the analysis, we want to briefly explain how the experiments were conducted: we are going to immerse the IRONsperm samples into very few milliliters of water. It allows, anyway, to have a very large bench of samples to inspect in order to find the "good swimmers" to extract data from. Moreover, it is important to highlight a particular behavior of the samples: it is possible to identify that some robots swims forward and some others swims backwards. At this stage, it is not considered as a problem because, even though we prefer a forward swimming direction, this factor does not influence the results.

A second important characteristic to mention is that the shape of the magnetic field is not changed during the experiments through the commands of the interface. In fact, the cone angle is fixed to 90° and the ellipsoidal shape is never assigned to the magnetic field in order to maintain a uniformity of the actuation within the workspace. Nevertheless, the roll, pitch and yaw angles of the magnetic field are constantly controlled in order to extract consistent data avoiding that external factors may interfere with the experiments.

Now that we have all the necessary information, we can proceed with the presentation of the results.
It is important to remind that we are investigating on the influence of the magnetization profile on the flagellar propulsion of the IRONsperm assuming that each configuration corresponds to a different magnetization profile, then we do not want to evaluate only the maximum results, but we want to derive conclusions from the trend over the whole frequency range in order extrapolate the characteristics provided by the groups of IRONsperm.

For the presentation of the results, we kept the classification into 15 configurations, but we categorized these profiles into four groups.

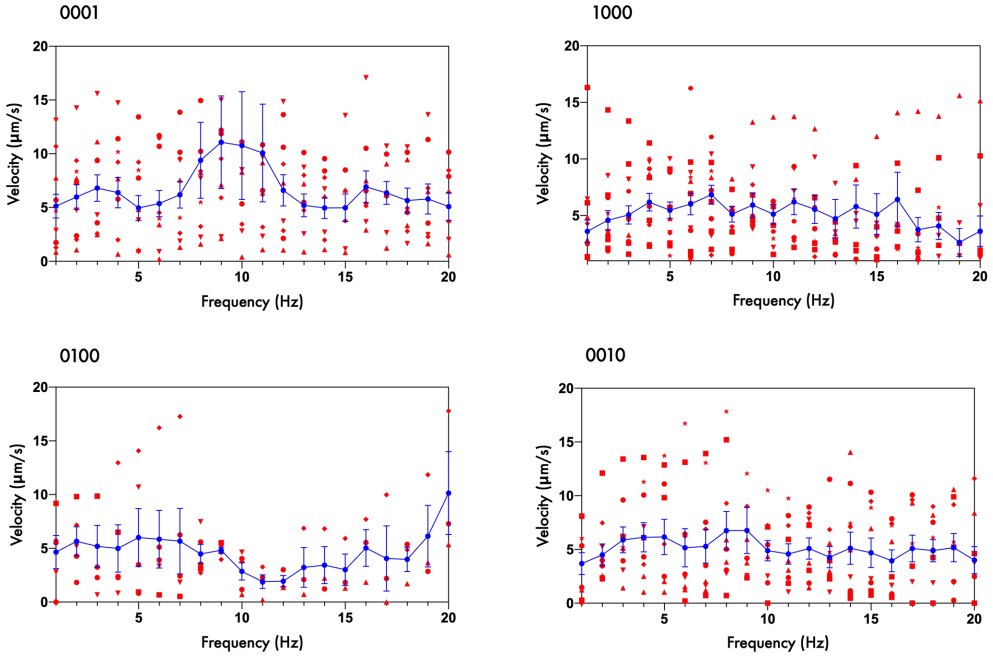

Figure 6.1.
Group 1 results: Characterization of the frequency response of configurations (reading from top-left row by row) 0001, 1000, 0100, 0010

The results presented in the figure correspond to the group 1. This group assembles the configurations that presents only one dipole magnetic moment. It means that the configurations considered are 0001, 0100, 1000, 0010. In these results, we evaluate the velocity performances out of the assigned frequency range: it is evident that they all present quite the same trend. Configurations 1000, 0100 and 0010 have a very similar behavior over all the considered frequencies and they swims with an average that is about 5 $\mu m/s$.

Differently from the other configurations, the 0001 group presents a better trend. In fact, it returns higher performances in the mid frequencies. This result confirms how the swimming behavior of the IRONsperm is strongly influenced by the magnetization profile and by the choice of the frequency of the external rotating magnetic field.

The phoenomenon is much more evident in the configurations associated to the group number 2.

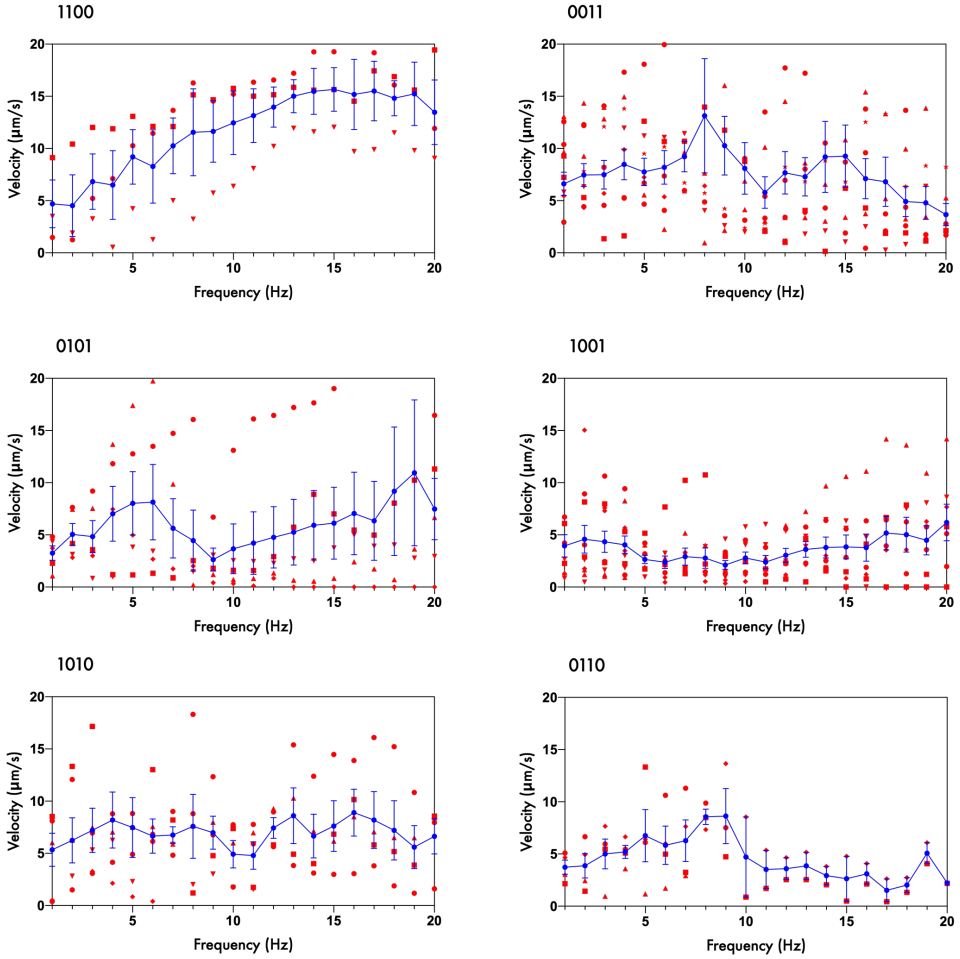

Figure 6.2.
Group 2 results: Characterization of the frequency response of configurations (reading from top-left row by row) 1100, 0011,0101,1001, 1010, 0110

According to the definition given to the first group, the second one assembles all the configurations that present two dipole magnetic moments along the body. So, the configurations considered in this case are 1100, 0101, 1010, 0011, 1001 and 0110.

As anticipated, in this case is clearer the fact that the IRONsperm samples can assume a different behavior according to the frequencies window that you consider. For example, configuration 1100 returns results that are much more appreciable at the high frequencies than at low frequencies, and it is confirmed by almost all the trials verified for this group. Certainly, 1100 is the best swimming configuration of this group. For what concerns the other configurations, we can see that 1001, 1010 and 0110 present a very similar behavior that is not much significant for the final purposes of the project. Instead, group 0101 has a good performance especially at high frequencies even though it is not able to reach the results expressed by configuration 1100.

Finally, we can focus on group 0011: even though it looks to report good results, they are not much significant. In fact, the trend is not consistent, and it is highlighted by the fact that the results of the single trials are spread over the whole velocity range. This issue is more evident in groups 3 and 4. These latter are going to be analyzed basing on the following plots.

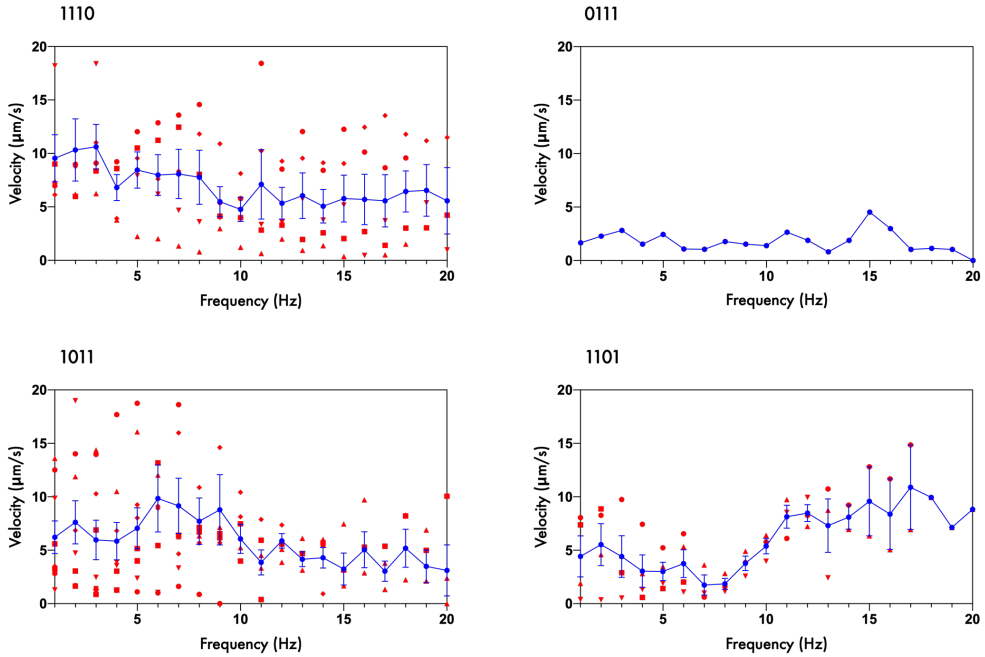

Figure 6.3.
Group 3 results: Characterization of the frequency response of configurations (reading from top-left row by row) 1110, 0111, 1011, 1101

Group 3 assembles configurations 1110, 1011, 0111 and 1101. These are the configurations that has three different dipole moments along the body of the sperm cell. Configurations 1110 and 1011 present the same problem that we identified for group 0011. The different behaviors of the samples belonging to the same configurations can be explained in the following way: the flagellar propulsion of the IRONsperm and, then, its motion are strongly influenced by the magnetization profile and his latter is characterized by the distribution of magnetic nanoparticles along the body of the cell. Since the average of the length of a spermatozoon is about 70 μm and the particles are in the order of nanometers, then two samples can belong to the same configuration and, at the same time, presenting two strongly different magnetization profiles. This phenomenon is really underlined by the huge standard deviation of these results. For this reason, we are considering the standard error of the mean in the presentation of our results and not the standard deviation: this method implies a normalization of the standard deviation out of the number of executed trials.

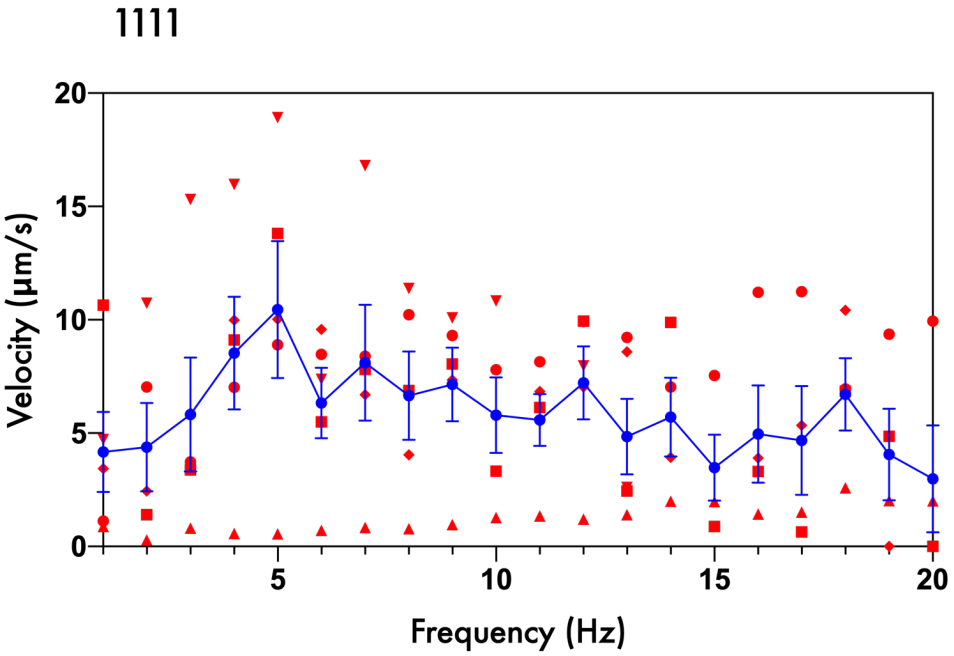

Figure 6.4.
Group 4 results: Characterization of the frequency response of configuration 1111

Group 3 and 4 are the poorest groups of this analysis, as confirmed by the last figure that represents the results obtained from group 4 (only configuration 1111). Configurations with three or four magnetic moments are the hardest to find and it was not possible to collect enough samples to obtain a consistent trend for these configurations. This is also a factor that contributes to the problem of not getting a consistent trend. In fact, if it is not possible to obtain congruent results with few trials, one of the methods that we adopted with other configurations was to extend the number of trials until the trend is consistent. Of course, this is not possible for these cases because there is not the chance to find a satisfying number of samples. These difficulties in capturing these IRONsperm profiles confirm the non-uniformity of the magnetization profile of the bovine sperm cells. The most evident proof of this problem is given by the results of configurations 0111. It presents only one trials because during the period of the experimental phase we found very few samples and only one good swimmer for this group.

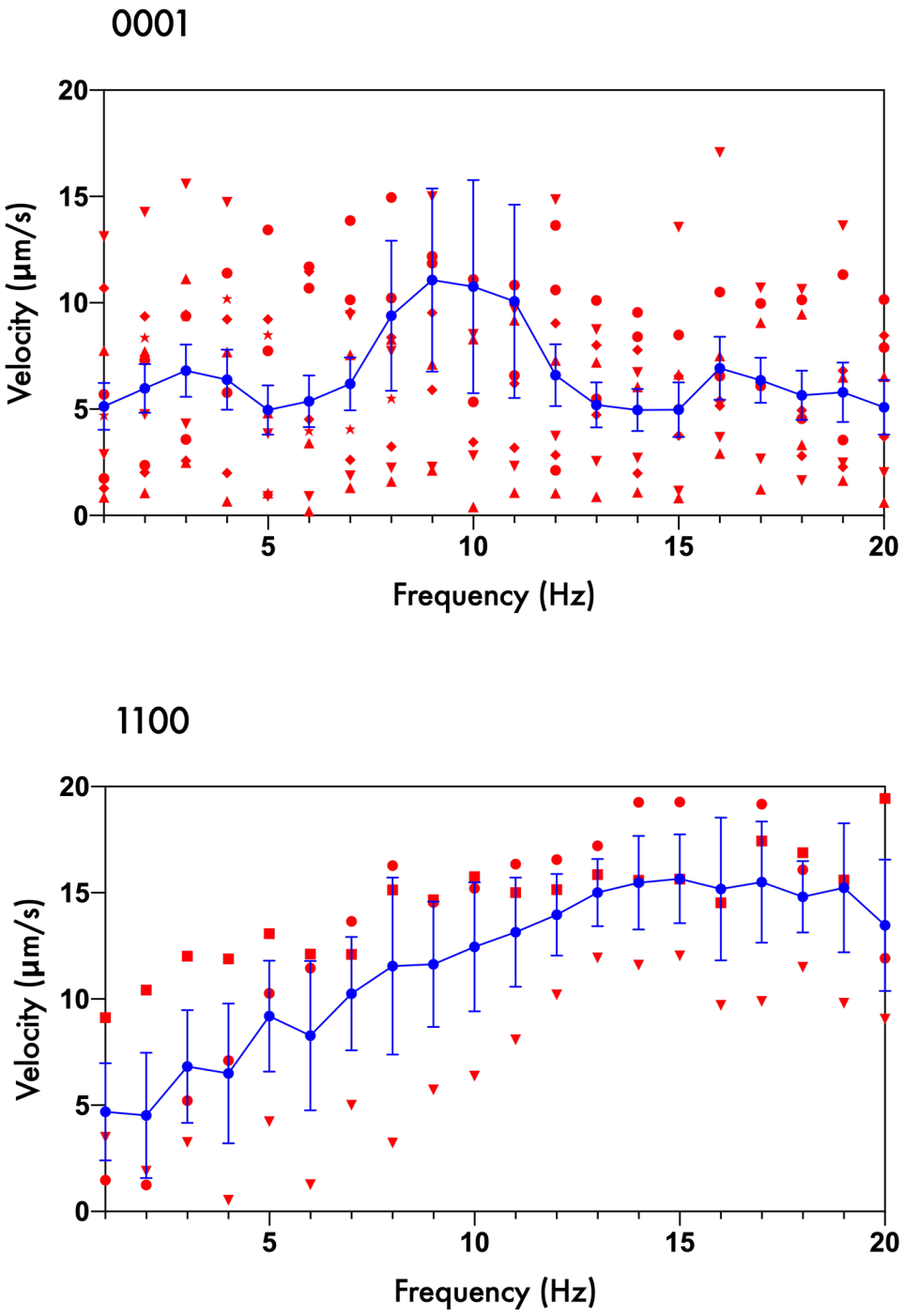

Figure 6.5. Best configurations according to experimental results (1100, 0001)

This experimental approach leads to the first considerations of the work reported in this thesis. This analysis confirmed the influence of the magnetization profile and the frequency of the external magnetic field on the actuation of the robot and then on its resulting motion. This experimental approach led to identify 0001 and 1100 as the best IRONsperm configurations: these results are provided by a sufficient

number of analysed samples and it came out that these two profiles assume the best swimming behaviour both in terms of maximum average speed and in terms of good performance over the whole frequency range.

6.2 Theoretical Results

The results that we have presented in the previous sections are important to evaluate the motion behavior of our micro-bio-robot, but they do not represent a satisfiable proof to take the final conclusions that we need to proceed with the next phases of the project. In fact, these results just provide some preliminary hints on the swimming behaviors of the configurations, but it is needed a countercheck to get consistent considerations to improve the final design of the IRONsperm.

We defined a mathematical hydrodynamic model of the IRONsperm that leads to characterize the waveform pattern and then to produce theoretical predictions on its swimming speed.
The wave-variables are used to dictate the time-dependent deformation of the flagellum of the robot. Due to design of this device, we have passive and active sections along the flagellum, depending on where the magnetic nanoparticles adheres on the sperm cell body. The objective of this analysis is to highlight and confirm, according to the previous results, what are the configurations that returns the best performances during the motion.

This represents another approach to investigate on the influence of the magnetization profile on the flagellar propulsion of the IRONsperm. In fact, as we have seen for Eukaryotic bacteria, actuation must be well distributed along the flagellum in order to obtain an efficient propulsion. Each configuration presents a different distribution of rice particles that results in a different magnetization profile and this is why we can derive properly our conclusions using this analysis too.

Before of introducing the results produced using the waveform analysis, we need to clarify that to extract the data we used the recordings of the good swimmers identified during the experimental analysis. We collected the videos that allowed to clearly recognize the flagellar propulsion during the swimming motion for each frequency and configuration. From these videos, we extracted a number of frames that included at least five beat cycles of the robot. This is where the real analysis starts: in fact, these frames were used to track the flagellum during the motion as we can see from the figure below.

Figure 6.6. Extracting data from IRONsperm flagellar deformation for waveform analysis

Assigning the right scale factor to each frame, we could derive the tangent angle $\phi(s)$ that characterizes the flagellar propulsion of the IRONsperm. Once that we know the value in function of the arc length s, then we know the waveform pattern along the whole body of the micro-bio-robot. We want to highlight the fact that the results are presented removing the dependence from the dimension of s and introducing, instead, the dimensionless quantity s/L.
As it was described in section 5.2, from this information it is possible to extract the three main parameters that define the deformation of the flagellum of the device. These parameters are the mean flagellar curvature K_0, the amplitude of the bending moment A_0 and the wavelength of the principal flagellar bending wave λ.

From the results that we are going to show, analogously to the previous analysis, we can derive some considerations on the best configurations to keep and the worst configurations to discard, for the final design purposes of the robot. The ideal behavior of the parameters will be used to evaluate the data extracted from all the configurations. As we have done during the characterization of the frequency response, the analysis will proceed using the new groups categorization. Finally, it is important to remember that all the data are derived from spermatozoa which are moving in close proximity to air surface, and the assumption is made that these figures also apply to spermatozoa moving freely in a bulk of fluid.

The first group of results to analyze is the mean flagellar curvature associated to the configurations belonging to group 1.

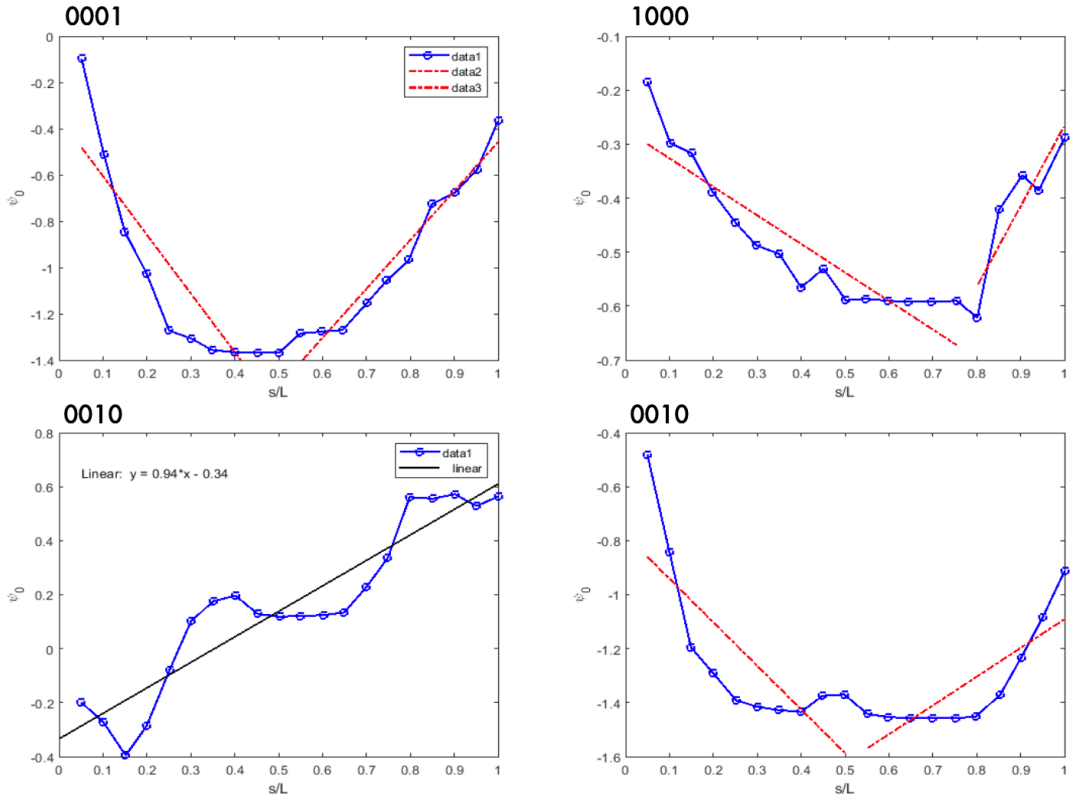

Figure 6.7.
Waveform Analysis: Mean flagellar curvature of the configurations belonging to Group 1 (Red and black lines represents the fitting curves)

This parameter returns a measure for the asymmetry of the mean shape of the flagellum. Ideally, if the waveform is symmetric, then the cell moves along a line. In real cases, bovine sperm cells hardly exhibits a symmetry in the plane of beating and it can be measured by fitting a line $K_0 s$.
In the proposed results, we can see that only the configuration 0001 returns curvature of the flagellum that resembles the ideal case. In fact, the ideal case is when the tangent angle $\phi(s)$ is equal to $K_0 s$ and it means that the flagellum is curved in a perfect arc with constant curvature K_0. It suggests the fact that the trajectory of the samples belonging to configurations 0001 presents a non-zero curvature.

Analogously, we can show the results of the second group where we have the six configurations with two dipole magnetic moments.

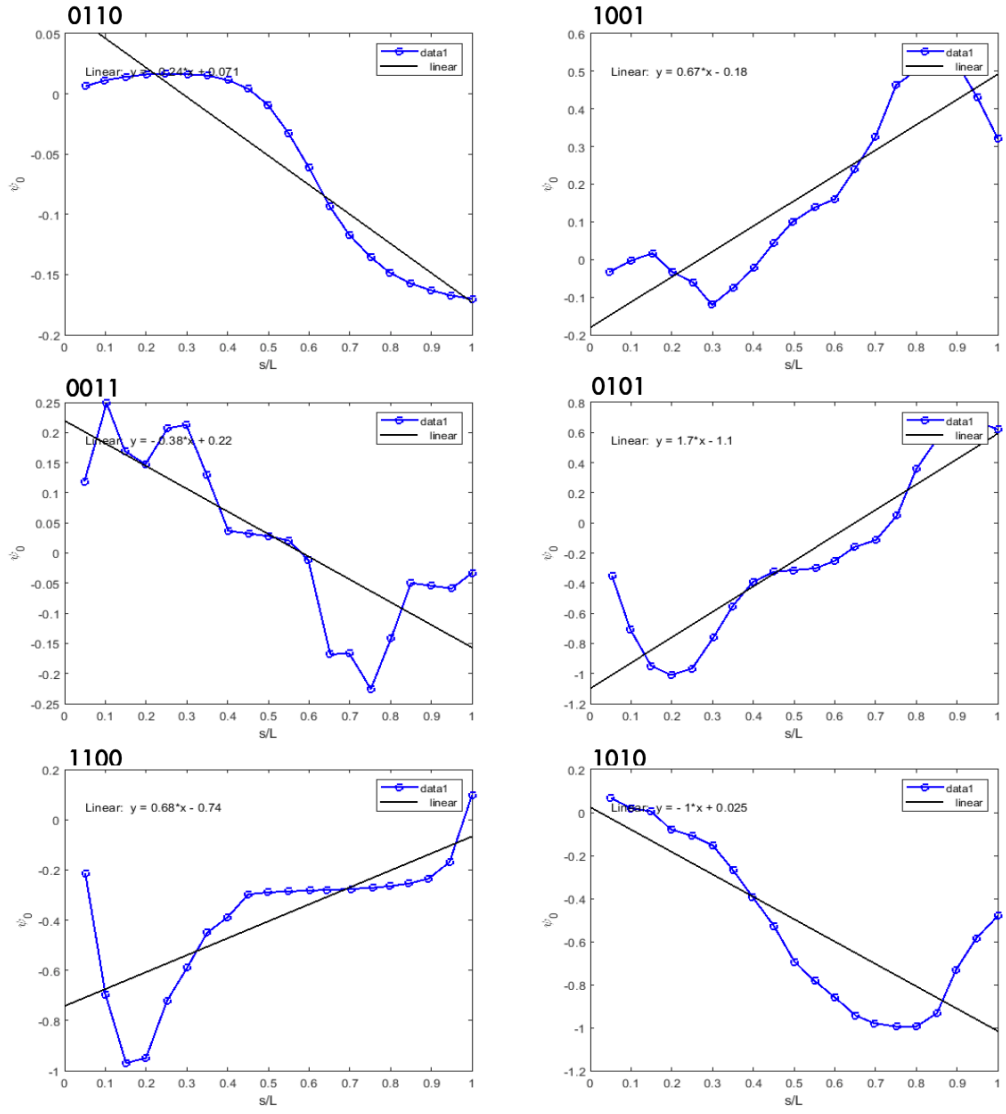

Figure 6.8.
Waveform Analysis: Mean flagellar curvature of the configurations belonging to Group 2 (Black lines represents the fitting curves)

These results do not seem to provide an ideal behavior from any of the considered configurations. Anyway, this parameter gives information just about the flagellar deformation of the robot that implies a non-straight swimming path. Hence, these results only contribute to indicate which of the IRONsperm profiles is more reliable when we need to track a specific trajectory.

As for group 2, also for group 3 and 4 we cannot extract many information from the results related to this parameter.

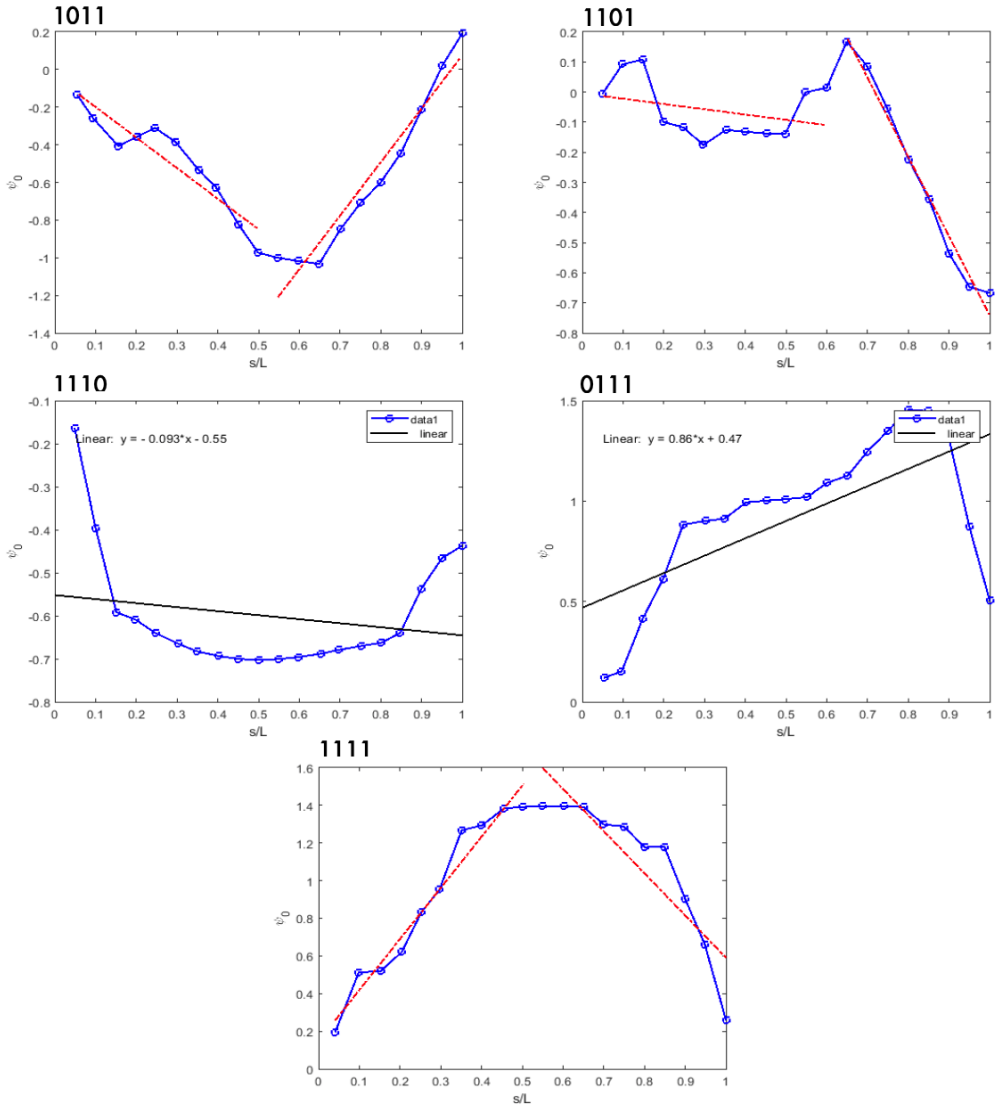

Figure 6.9.
Waveform Analysis: Mean flagellar curvature of the configurations belonging to Group 3 and 4 (Red and black lines represents the fitting curves)

It is possible to see that configuration 1111 gives results very similar to the one that we examined for configuration 0001.

Even though the mean shape of the flagellum is expected to depend only on the asymmetric architecture of the flagellar components, in [6] it was proved that it is influenced by the viscosity of the fluid where the sperm cell swims in. It means that the flagellar asymmetry is an emergent property that depends on active processes within the flagellum.
Now, we can move on to analyze the results produced by the derivation of the amplitude of the bending moment A for each configuration. We start again from the group 1.

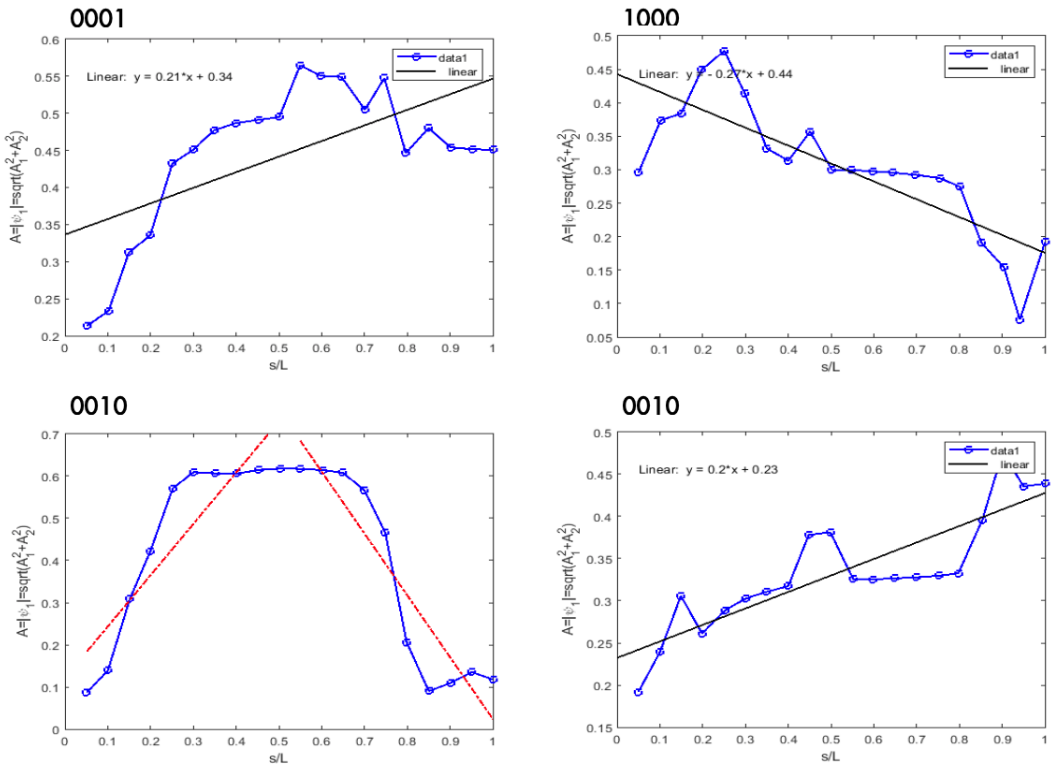

Figure 6.10.
Waveform Analysis: Amplitude of the bending moment of the configurations belonging to Group 1 (Red and black lines represents the fitting curves)

Even in this case, we comment the presented results basing on the definition of the ideal case for this parameter. It occurs when the bending amplitude increases linearly along the flagellum and it is defined as $|\psi_1(s)| = A_0 s$. It can be evaluated by fitting the line $A_0 s$, and the considerations are very similar to the one taken from the curvature results. Even in this case the best samples seem to be the one belonging to group 0001 since they present a linear increase, as desired. Contrarily, 1000 and 0010 are the worst cases because the first one returns a linear decrease of the amplitude whereas in the 0010 there is not monotony and it results in two opposite curves.

In the following figure, we can show the results corresponding to the configurations of the second group.

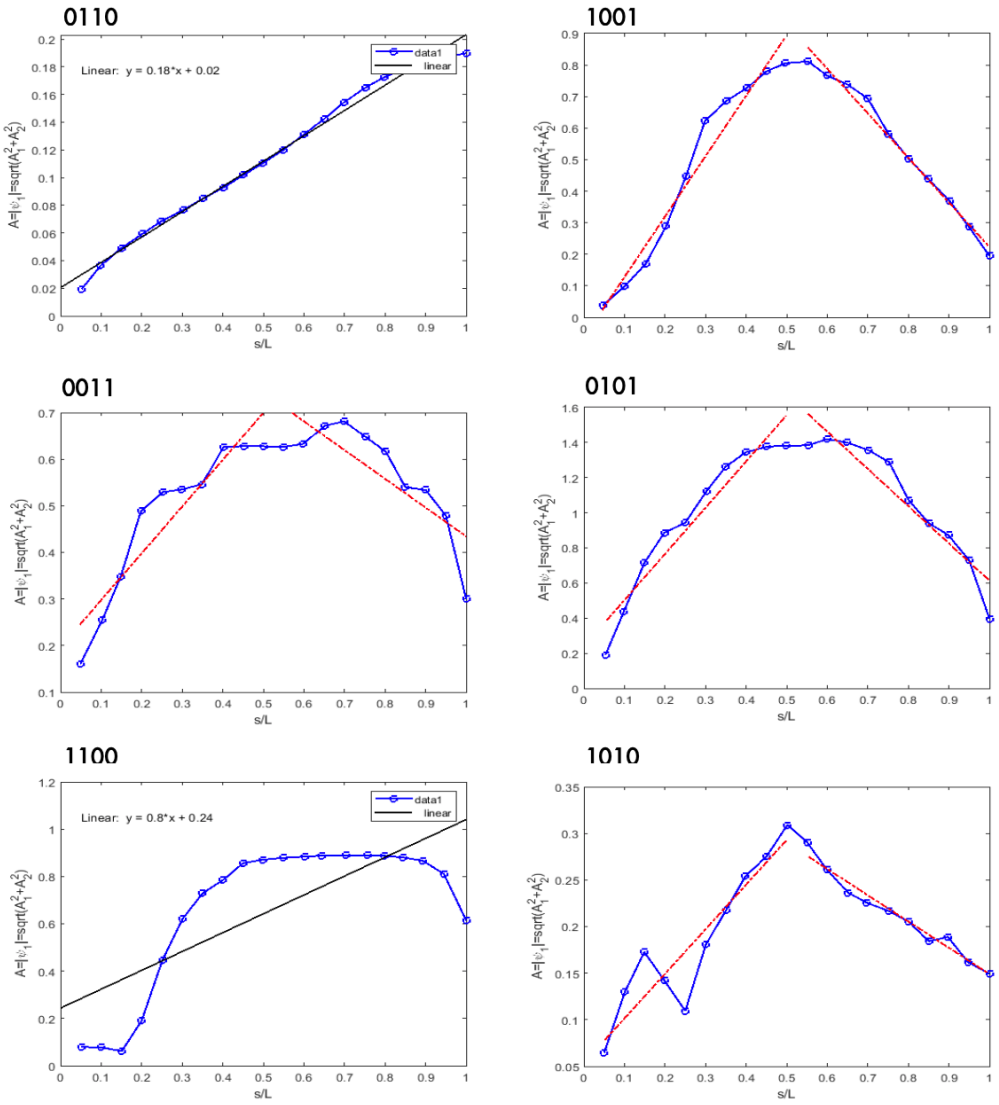

Figure 6.11.
Waveform Analysis: Amplitude of the bending moment of the configurations belonging to Group 2 (Red and black lines represents the fitting curves)

These results are very satisfying since they are exactly what we were seeking. In this group, the only configurations that returns a good behavior in the trend are the 0110 and 1100. For this latter, this is the first confirm from the waveform analysis to what we have concluded for the results obtained by the characterization of the frequency response.

Groups 3 and 4 once again do not return remarkable results. In this case, it is another confirm that explains that these configurations do not provide good swimmers and then they are very likely to be discarded.

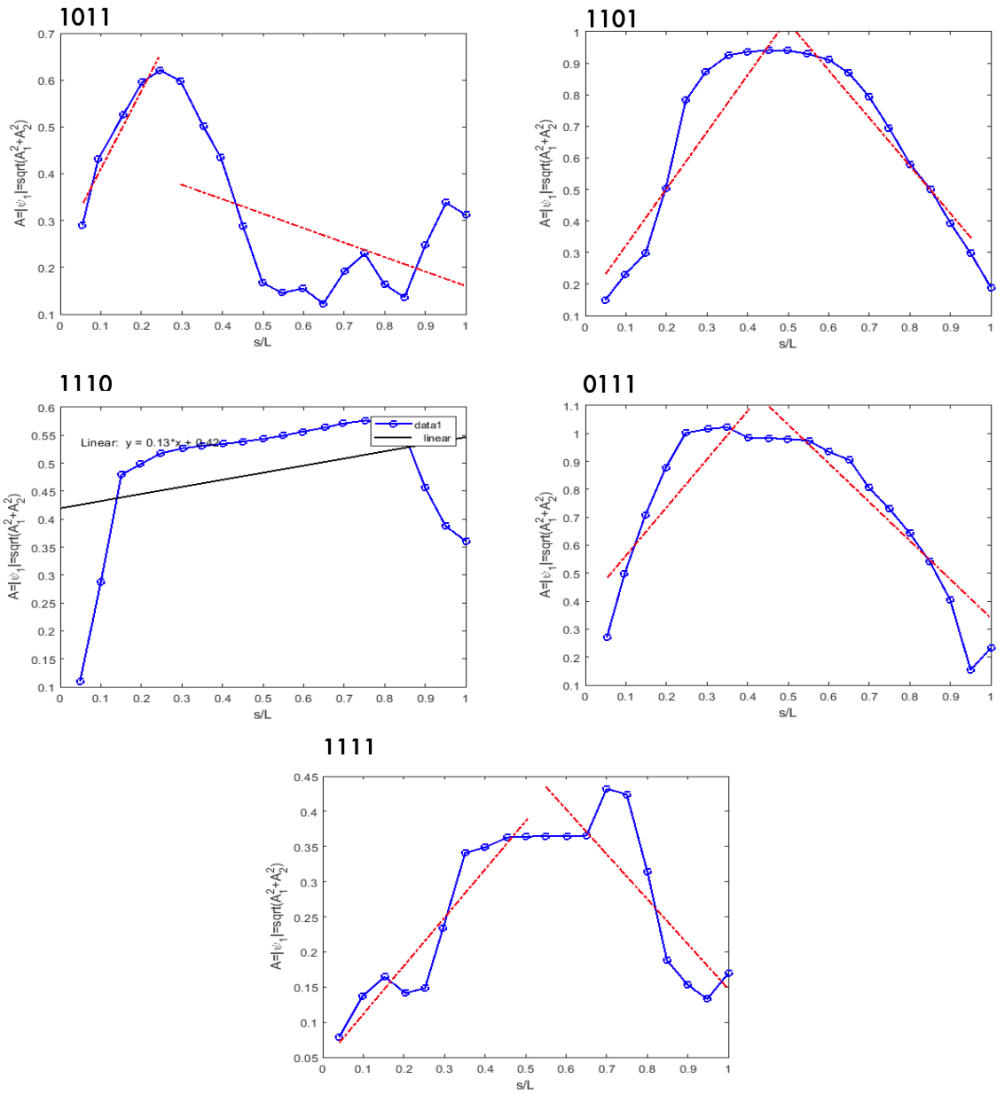

Figure 6.12.
Waveform Analysis: Amplitude of the bending moment of the configurations belonging to Group 3 and 4 (Red and black lines represents the fitting curves)

The last of the three parameters is represented by the wavelength of the principal flagellar bending wave. This value can be extracted by computing the phase angle $\Phi(s) = -arg(\Psi(s))$. For this case, contrarily to the previous ones, we are not going to evaluate the ideal behavior of this parameter to compare it with our results. Instead, we are going to analyze the trend of the phase angle since this value is important because it characterizes the progression of the wave along the flagellum of the IRONsperm.

Once again, we start by presenting the results obtained for the configurations that belong to group 1.

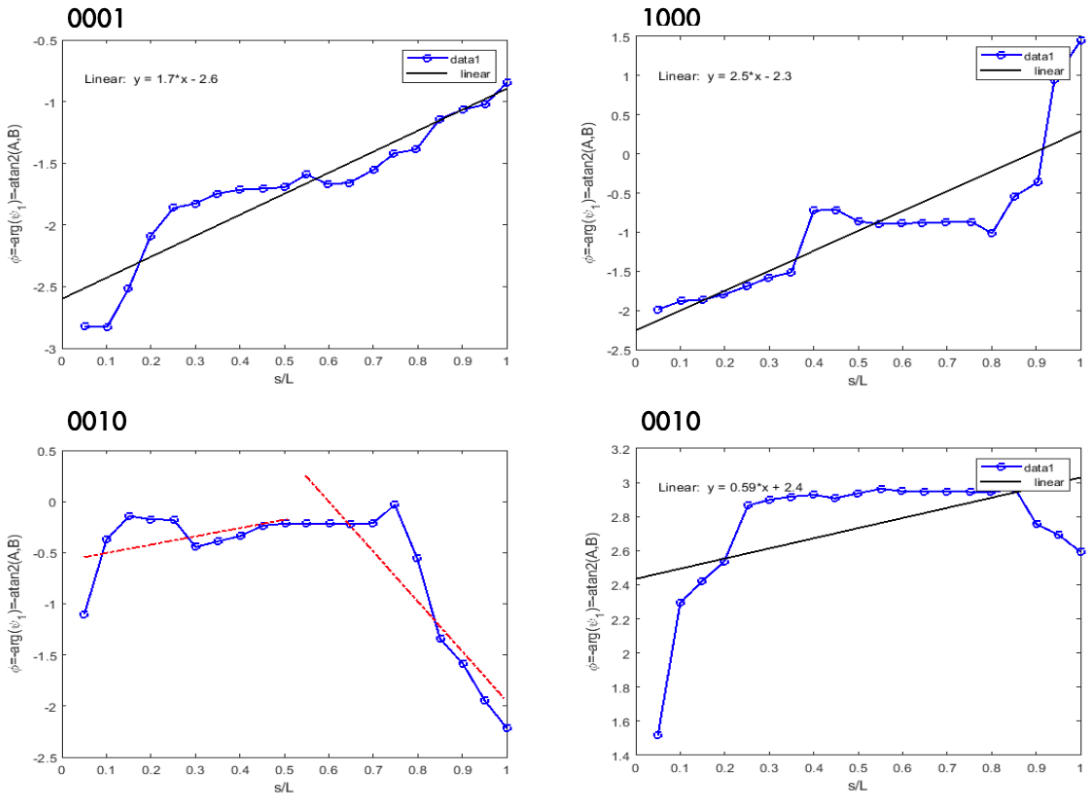

Figure 6.13.
Waveform Analysis: Wavelength of the principal flagellar bending wave for the configurations belonging to Group 1 (Red and black lines represents the fitting curves)

In this group, the relevant results are provided by the configurations 1000 and 0001. This latter once again confirms our expectations. These two groups, in fact, shows a progression of the wave from the head of the sperm cell to the distal end of the tail, or the opposite. An example of a bad progression is provided by group 0010 where two waves are generated, and they travel opposite to each other and it implies a mutual annihilation during the motion.

In the next figure, it is possible to make some considerations of the progression of the wave that characterizes the configurations of the second group.

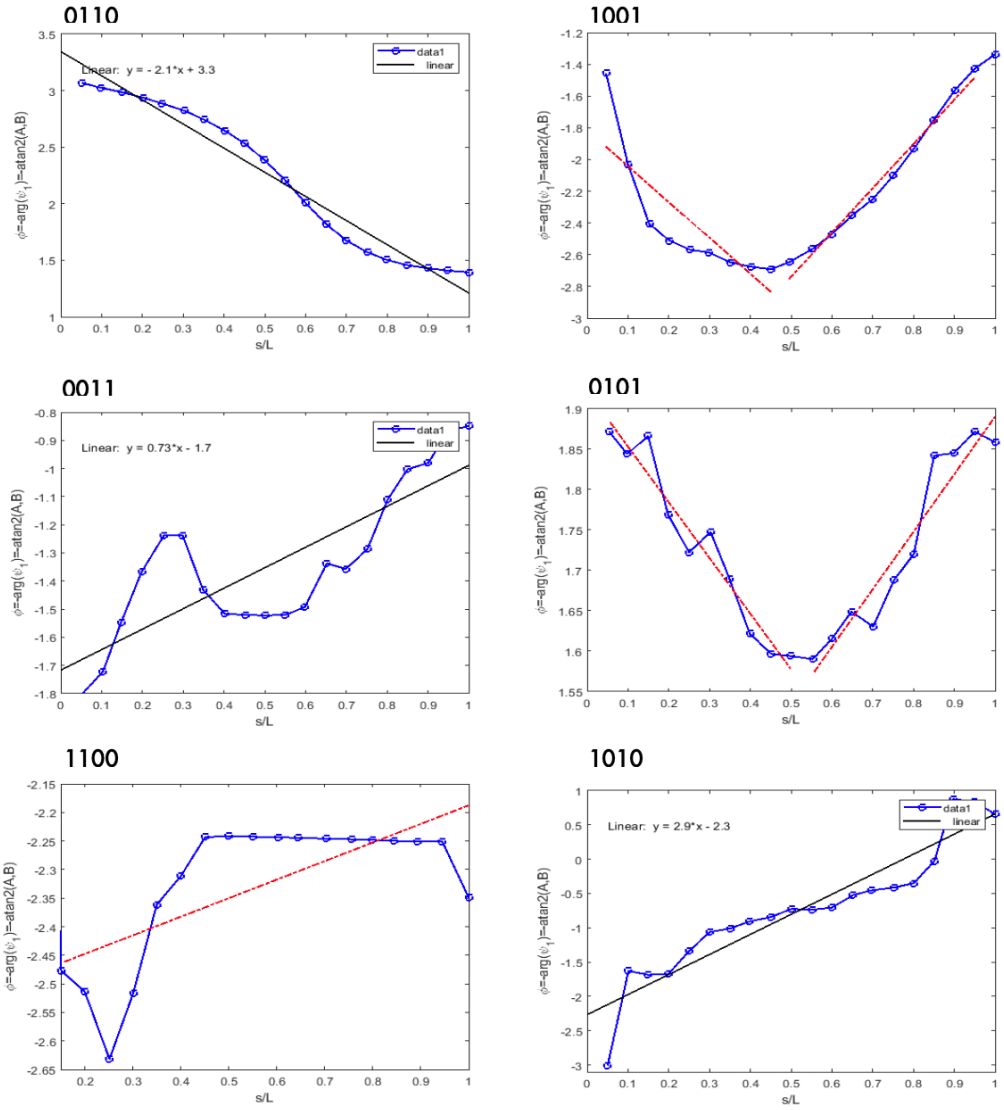

Figure 6.14.
Waveform Analysis: Wavelength of the principal flagellar bending wave for the configurations belonging to Group 2 (Red and black lines represents the fitting curves)

The only really bad configurations of this group are 1001 and 0110. In fact, they present, as for 0010, two opposite waves during the swimming motion. Instead, the configurations that present a good progression are, also in this case, 1100 and 0110. This latter is important since it is the only configuration that reproduces the natural waveform of the sperm cell.

In the next plots,we give an overview of the phase angle results for group 3 and 4. They return strange progressions of the wave along the flagellum. This can be caused by "too much actuation": if the sperm cell is coated by too many magnetic nanoparticles then it can result in an asynchrony during the motion of the active section of the micro-bio-robot.

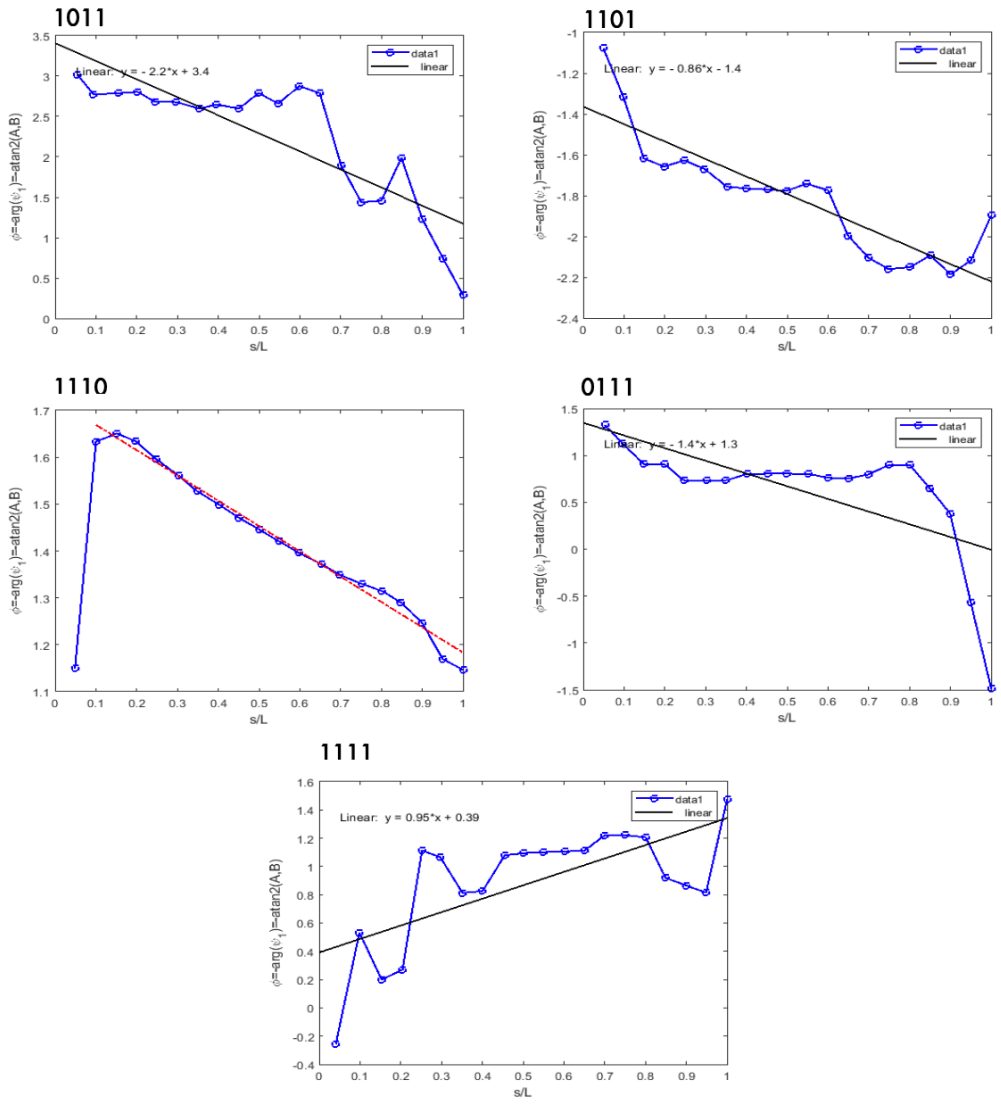

Figure 6.15.
Waveform Analysis: Wavelength of the principal flagellar bending wave for the configurations belonging to Group 3 and 4 (Red and black lines represents the fitting curves)

From these results we can also conclude that, generally, when we have particles on the principal pieces then the resulting trend tends to generate two waves that travel along opposite directions and the net thrust decreases.

In the next table, we are going to show the numerical data obtained for the three parameters that were presented in this section:

Group	*k* [rad/mm]	*A* [rad/mm]	*Lambda* [um]
G0001	39,1	3,5	221,7
G1000	16,8	4,5	150,7
G0010	15,6	22,3	209,4
G0110	4	3	179,5
G1001	11,1	27,7	149,3
G0011	6,3	13,5	516,4
G0101	28,3	39,5	537,6
G1100	11,3	13,3	191,4
G1010	16,6	6,3	129,9
G1011	37,2	16,4	171,3
G1101	23,3	27,6	438,3
G1110	1,5	2,1	698,2
G0111	14,3	25,9	269,2
G1111	41,2	11,04	396,8

These results are important for different reasons. Under the perspective of this work, we need the values of the three parameters to predict, using Resistive Force Theory, the propulsive thrust exerted by the flagellum during the motion. This analysis will be explained in section 6.3, and we will describe the procedure that we want to follow in order to compare these results, predicted using the waveform analysis measurements, with the ones that can be computed using the experimental data collected during with the characterization of the frequency response. These results can be used also for other purposes: it will not be subject of this thesis, but during the analysis we found out that there is a direct correlation between the choice of the wavelength and the magnetization profile. In fact, choosing a certain value of λ it is possible to get the deformation of the flagellum that corresponds to a specific magnetization profile. These results are important for future design and control purposes of the IRONsperm.

6.3 Discussion of the Results

The previous sections concerned the analysis of the motion of the groups of self-assembled micro-bio-robots. As we have presented in this thesis, the approach proposed to generate these devices was magnetizing the passive flagellum by doping it with nanoparticles. It resulted in an organic body with lumped thin layers of magnetite. Since the surface charge of the cell dictates the location of the nanoparticles and assuming that this charge is not uniform along the body, then the magnetic layer varies across the cell. It leads to the determination of distinct magnetization profile along the flagellum.

In this work, we proposed to investigate on the influence of the magnetization profile on the flagellar propulsion of the IRONsperm. For this concern, we sectioned the sperm cell body into four parts, and we identified 15 configurations where each corresponds to a particular magnetization profile that produces a distinct motion behavior. The evaluation of this behaviors leads to the definition of the design and control features that we want to focus on in the future developments of this work. In this chapter, we explained how we derived our conclusions adopting two methods that offer two different perspectives to evaluate the problem. We exploited these two approaches in order get significant results for our analysis and, moreover, to introduce new informations that may open new scenarios for future analysis.

This work of analysis led to define two independent set of results, one for each methos. In particular, the characterization of the frequency response identified 1100 and 0001 as the best configurations in terms of maximum average speed and trend over the whole frequency range. The waveform analysis, in this discussion, was used as counterproof to confirm or discard the results obtained during the experimental phase. This theoretical approach offered a vision of the micro-bio-robot under a different point of view: the parameters that we computed described the wave pattern characteristics of all the configurations and, once again, 1100 and 0011 were identified as the best profiles. Even though the results of the two procedures were produced and evaluated independently on each other, they both have a lot of potentialities to derive new important information for the study of the IRONsperm. In this final section, we are going to introduce the next analysis to develop and how to combine the set of results that we already computed. Using the deformation measurements and the waveform parameters computed during the waveform analysis it is possible to derive the propulsive thrust produced during the motion by each configuration.

To achieve this aim, we use the Resistive Force theory that can be simplified as follows:

$$f_f = \xi_t V_t + \xi_n V_n$$

where ξ_t and ξ_n are, respectively, the tangential and the normal components of the drag force exerted on the body of the cells expressed as two constant values. These latter can be computed as:

$$\begin{aligned} \xi_t &= \frac{2\pi\eta}{l_n\left(\frac{2\lambda}{r_f}\right) - 1/2} \\ \xi_n &= \frac{4\pi\eta}{l_n\left(\frac{2\lambda}{r_f}\right) + 1/2} \end{aligned}$$

where r_f is the radius of the flagellum and η is the fluid viscosity equal to 1 mPa. The velocity components along the body of the cell can be computed in function of $r(s,t)$ that is the steady-state solution of the dynamic model of the robot and it characterizes the deformation of the hybrid device:

$$r(s,t) = \int_0^s (cos(\phi)e_1 + sin(\phi)e_2)\, ds$$

where $e_1(t)$ is the propulsion axis of the robot and $\phi(s,t)$ is the tangent angle.

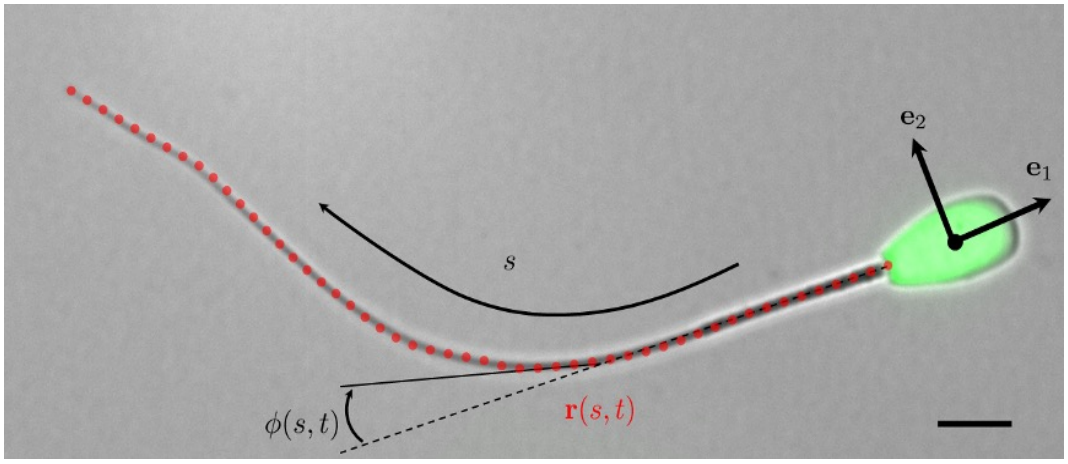

Figure 6.16. IRONsperm propulsion formalization.

It is possible to derive the velocity components basing on the kinematics of the flagellum at any point of the arc length s:

$$\begin{aligned} V_t &= (\dot{r}(s,t) \cdot t(s,t))\, \mathbf{t(s,t)} \\ V_n &= \dot{r}(s,t) - V_t \end{aligned}$$

where $\dot{r}(s,t)$ is the time derivative of $r(s,t)$ and $\mathbf{t(s,t)}$ is the local tangent vector. This analysis leads to the computation of the force exerted by the flagellum during the propulsion in a fluid characterized by a viscosity η. The following images report the force contours of each IRONsperm configuration, according to the data obtained from the waveform analysis:

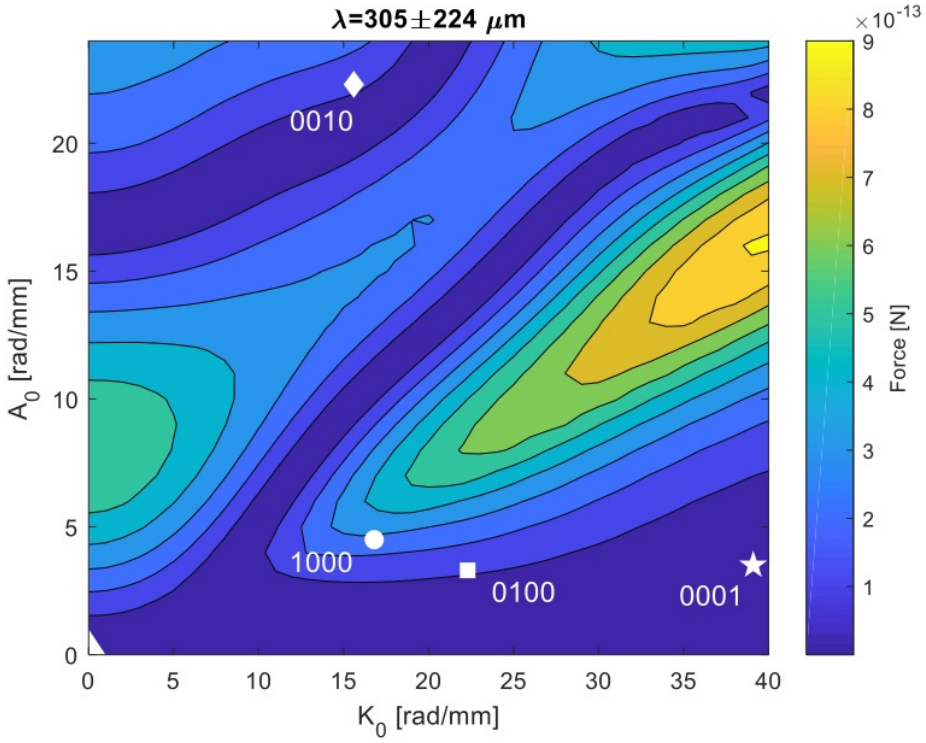

Figure 6.17. Force Contours for Group 1.

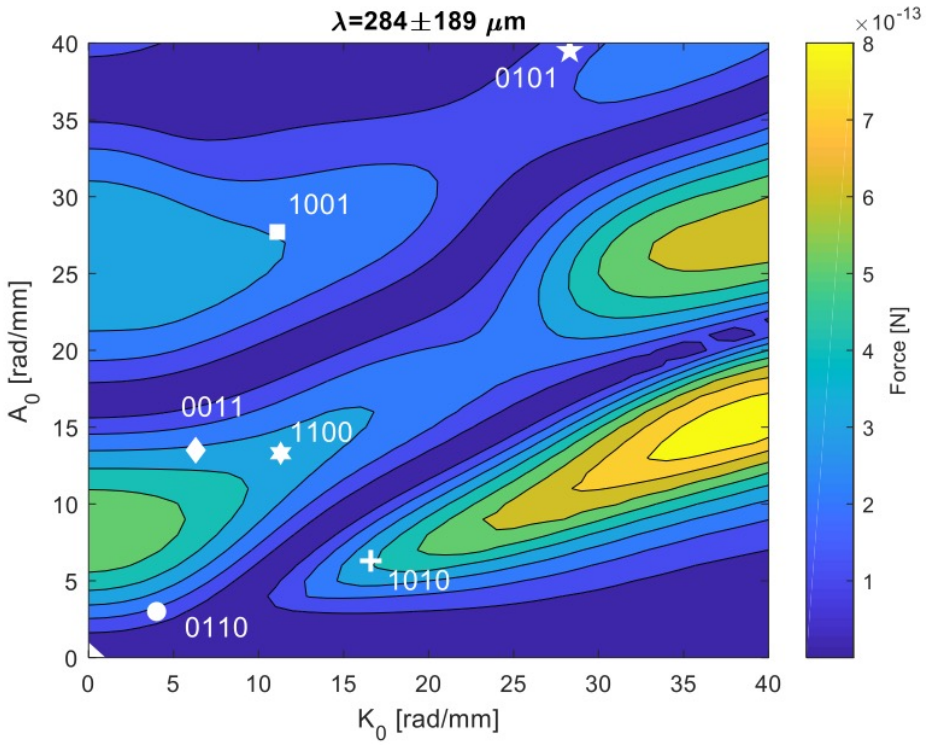

Figure 6.18. Force Contours for Group 2.

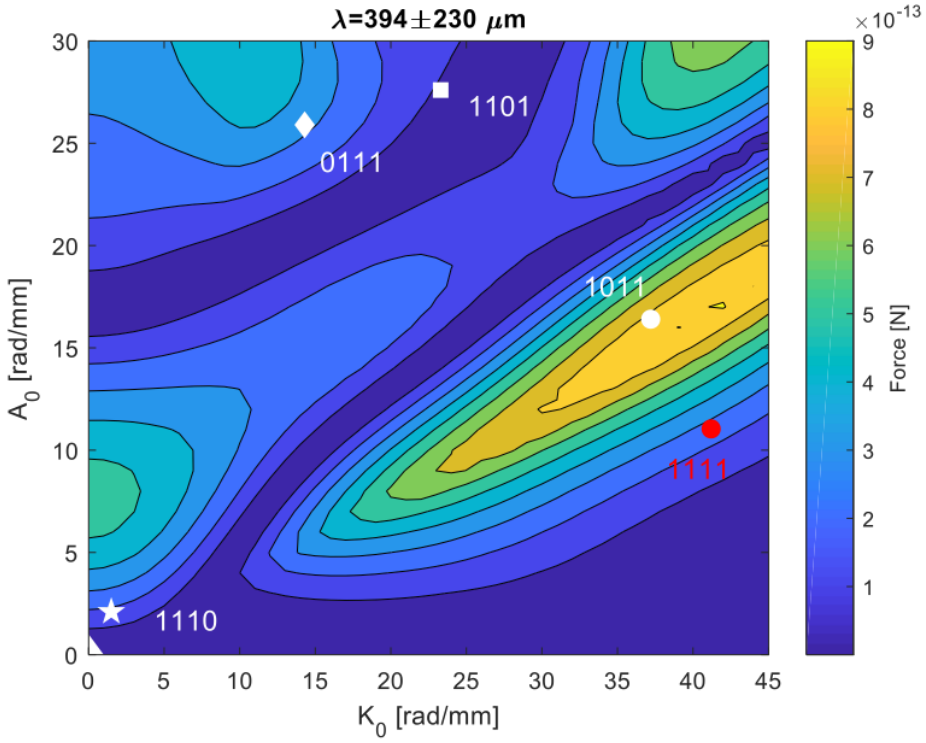

Figure 6.19. Force Contours for Group 3 and 4.

These graphs were reproduced by computing an average wavelength for all the profiles in the considered group. These are the first results that we produced through this force analysis. The main finding is that as the number of coated segments increases also the propulsive thrust increases. These theoretical predictions suggest that 1111 configuration is the one that produces the highest thrust. This conclusion does not seem to agree with the results obtained during the experimental data. This is why we want to combine these results: our aim is to produce the thrust exerted by the robot during the motion using the experimental data that we already collected. The final combination of these results will provide a new perspective to evaluate the IRONsperm profiles and it will open new scenarios for the next evaluations.
The comparison with the experimental data can be produced adopting the following model:

$$f_f + f_h = 0$$

where f_f is the force produced by the flagellar propulsion computed through the data extracted by the waveform analysis and represented on the force contouurs. Whereas, f_h is the force exerted by the head during the motion that we want to compute using experimental data.
In order to derive this results, we need to assume that the head of the sperm cell is a perfect sphere, such that:

$$f_h = 6\pi\eta r_h V$$

where r_h is the radius of the head equal to 10 μm.

The results of this procedure are not reported since we consider them too unripe to be presented and we are not still able to derive significant conclusions on these. We presented this procedure in order to show how this analysis is supposed to proceed in the closest next steps and what we expect to investigate on. The analysis of the force and the comparison between the experimental data and the predictions will lead to a deeper analysis of the flagellar propulsion of the IRONsperm and to an evaluation of the influence of the external factors that modify the swimming behaviors of the robots.

Chapter 7

Conclusion

This master thesis project represented the first concrete step of a very ambitious project whose aim is to use a new microrobotics device called IRONsperm for localized drug delivery, in particular, to graft anti-cancer drugs in a region of interest.

This work introduced the design of a new micro-bio-robot: the IRONsperm is a hybrid device generated by the adhesion of ferromagnetic nanoparticles and the bovine dead sperm cells. The electrostatic attraction between the positive charge of the particles and the negative charge of the biological cells allowed to create our robot. The surface charge of the cell and the nanoparticles and their spatial orientation are important factors in the determination of the magnetic layer along the cell. The net surface charge is indicative of the total amount of nanoparticles that coat the cell, whereas the spatial orientation of the cell and the surrounding nanoparticles influence the location of the magnetic layer. One of the most important characteristics of the bovine sperm cell that was exploited in this work is represented by the the magnetic charge that is not uniform along the flagellum. This characteristic implies that the distribution of particles is not uniform along the sperm body and it is unpredictable which segments will be coated. For this reason, we divided the IRONsperm body into four sections (head, mid-piece, principal piece, distal end) such that we can distinguish fifteen different configurations of the same robot and we can seperately analyze all the groups independently from each other.

Different configurations produce different combinations of magnetic moments along the body of the sperm cell, and it corresponds to obtain different magnetization profiles. This categorization is one of the main aspects that explains why the principal aim of this work is to investigate on the influence of the magnetization profile on the flagellar propulsion of the IRONsperm.

During this work, it resulted that the distribution of the nanoparticles on the body of the biological cell plays a fundamental role in the motion behavior of the robot. In fact, a particular distribution leads to a characteristic deformation of the sperm cell body that is strongly related to the magnetization profile. These latter produce different behaviors and it results in an actuation of the robot, achieved through the application of an external magnetic field, that presents different charac-

teristics for each group.
Moreover, during the analysis proposed in this work, it was highlighted the fact that the distribution of the particles can lead to a different motion behavior even between samples belonging to the same configuration. This problem produced unexpected issues during both the experimental and the theoretical analysis: for this reason, we needed to find several ways to figure it out and get a consistent and satisfying set of data in order to produce reliable results that led to important conclusions without any ambiguity. The method that allowed to minimize this problem was to increment the experimental extraction of data in order to derive results whose trends is justified by the average of several samples.

The analysis elaborated in this project aimed at characterizing the motion of each group of IRONsperms in order to derive relevant considerations for design and control purposes. The main strategy to achieve this aim was to develop a system of analysis that led us to identify the best IRONsperm profiles, such that they can be used in the future procedures of the project.
We have shown in this report that we proceeded using two different approaches: an experimental analysis and a theoretical method. The former gave us the opportunity to get direct observations on the motion behavior of the micro-bio-robot. This phase required time to be improved and after important efforts we found the good strategy to use the electromagnetis system to drive the robots. To avoid near-surface effect on the helical propulsion, the axis of rotation of the applied magnetic field is controlled to have a non-zero pitch angle (angle with the horizontal plane). This angle enables the samples to swim upward away from the surface and from the nanoparticle aggregates. Once located away from the solid boundary of the reservoir, the maximum average speed of IRONSperm samples is measured for frequency range of 1 to 20 Hz. Thanks to the characterization of the frequency response that we conducted on all the groups, we were able to provide a first overview of the different swimming characteristics of all these robots. This experimental procedure gave the opportunity to have a direct observation of the motion behavior of the IRONsperm samples. It was fundamental to have a first reflection of the different swimming mechanisms adopted by the different profiles and it allowed to carry on an in-depth analysis which gave us the chance to better understand and control these devices during the motions using our experimental setup. Thanks to this procedure, we collected a huge amount of data that can be adapted to different kind of analysis. Even though they are not versatile as the waveform analysis results, they can be used in order to evaluate design and control features of the IRONsperm. An example was shown in section 6.3, where we explained how to exploit these data in order to conduct an analysis on the propulsive thrust generated by the robot and to compare the results with the expectations obtained through the Resitive Force Theory.

Our second approach was represented by an analysis of the waveform pattern produced by the robot during the motion. This is a theoretical method that implies the simulation of the motion of the sperm cell using a numerical model: this way, it was possible to extract three main parameters that gave us a huge amount of information on the wave propulsion of each group.
As the experimental analysis did not provide only the results of the characterization of the frequency response, also this method did not limit itself to produce only the

three final parameters. In fact, thanks to this analysis we had the chance to introduce new aspects of this robot that will form a strong base for the future analysis. We identified a connection between the value of the wavelength of the principal flagellar bending wave and the magnetization profile of the robot. This information can be exploited in the next phases of the project to focus on the development of a specific design of the robot.

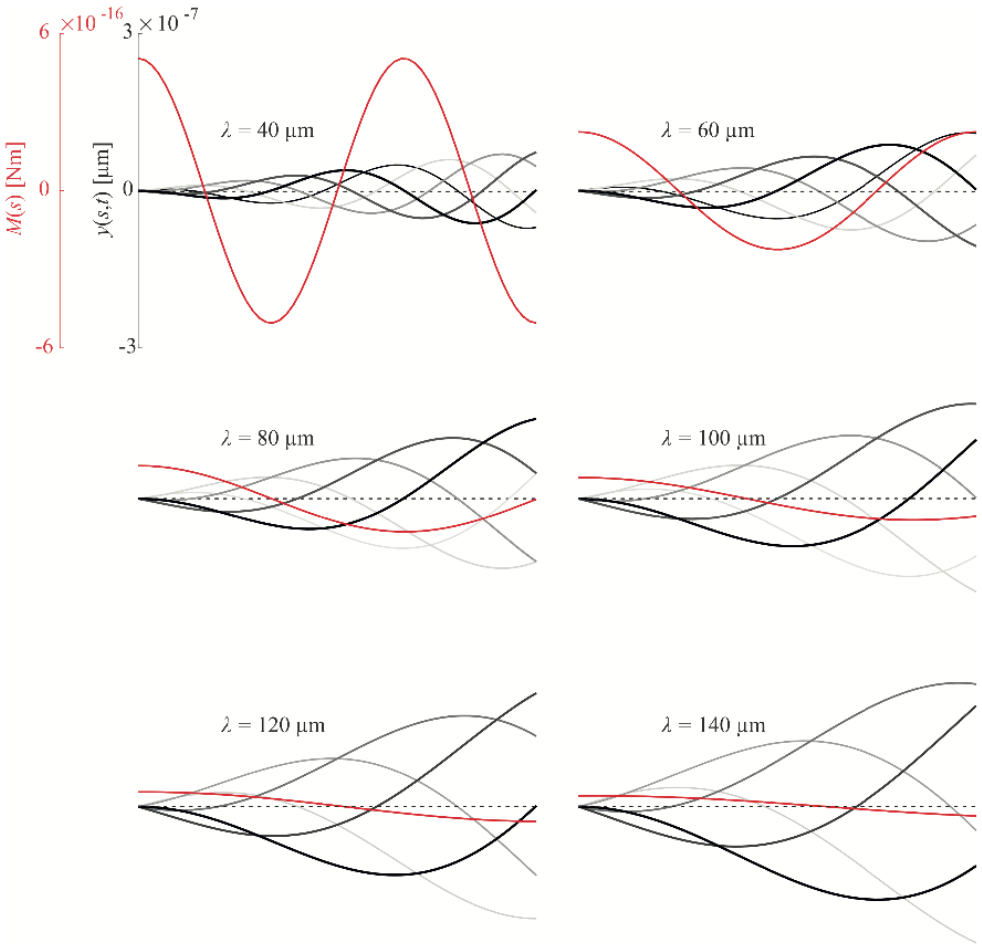

Figure 7.1. Connection between flagellar deformation and wavelength.

Thanks to the derivation of these parameters, now it is also possible to define the perfect length of the tail of the robot, in order to obtain an elasticity that can produce the best propulsion of the robot. Another novel aspects that can be extrapolated from this analysis is the derivation of an accurate value of the elasticity that characterizes the sperm cell body: this value is not known and at the Surgical Robotics Laboratory, our collaborator are attempting to extract this value that might open new scenarios both in the engineering and in the biotechnology fields.

The combination of the results produced by these two approaches led to the

revelation of the ones that results to be the best configurations. These are the groups 0001 and 1100 and the comparison of the final results proved the consistency and the reliability of these analysis.
Thanks to this work, we expect to focus the future developments of the project on these two configurations. It will allow to proceed, firstly, with the motion control approach in order to implement a system that allows to control accurately the robot in real-time. Successively, all these results will contribute to the maturation of the project such that in vivo applications will be tested: these new steps of the research will include the introduction of the ultrasound imaging system to localize and keep track of the robot during the application into the human body and, also, to a deeper study on the charge mapping of bovine sperm cells. Thanks to all these elements, we will move closer and closer to the Cancer-relevant drug delivery with IRONsperm.

Bibliography

[1] Jake Abbott et al. “Robotics in the Small, Part I: Microbotics”. In: *Robotics Automation Magazine, IEEE* 14 (July 2007), pp. 92–103. DOI: 10.1109/MRA.2007.380641.

[2] Ricardo Cortez. “The Method of Regularized Stokeslets”. In: *Siam Journal on Scientific Computing* 23 (Dec. 2001). DOI: 10.1137/S106482750038146X.

[3] Ricardo Cortez, Lisa Fauci, and Alexei Medovikov. “The method of regularized Stokeslets in three dimensions: Analysis, validation, and application to helical swimming”. In: *Physics of Fluids* 17 (Feb. 2005). DOI: 10.1063/1.1830486.

[4] B. Crowell. *Fields and Circuits.* 2020.

[5] Lixin Dong and Brad Nelson. “Tutorial - Robotics in the small Part II: Nanorobotics”. In: *Robotics Automation Magazine, IEEE* 14 (Oct. 2007), pp. 111–121. DOI: 10.1109/MRA.2007.905335.

[6] B. M. Friedrich et al. “High-precision tracking of sperm swimming fine structure provides strong test of resistive force theory”. In: *Journal of Experimental Biology* 213.8 (2010), pp. 1226–1234. DOI: 10.1242/jeb.039800.

[7] J. GRAY. “Undulatory Propulsion”. In: *Journal of Cell Science* s3-94.28 (1953), pp. 551–578. ISSN: 0021-9533.

[8] J. GRAY and G. J. HANCOCK. “The Propulsion of Sea-Urchin Spermatozoa”. In: *Journal of Experimental Biology* 32.4 (1955), pp. 802–814.

[9] Mert Kaya et al. “Development of a Coil Driver for Magnetic Manipulation Systems”. In: *IEEE Magnetics Letters* 10 (2019), pp. 1–5.

[10] Islam S. M. Khalil et al. “Modeling of Spermbots in a Viscous Colloidal Suspension”. In: 2019.

[11] Islam Khalil et al. “Biocompatible, accurate, and fully autonomous: a sperm-driven micro-bio-robot”. In: *Journal of Micro-Bio Robotics* 9 (June 2014). DOI: 10.1007/s12213-014-0077-9.

[12] Islam Khalil et al. “MagnetoSperm: A microrobot that navigates using weak magnetic fields”. In: *Applied Physics Letters* 104 (June 2014), pp. 223701–223701. DOI: 10.1063/1.4880035.

[13] Islam Khalil et al. “Resemblance between motile and magnetically actuated sperm cells”. In: *Applied Physics Letters* 116 (Feb. 2020), p. 063702. DOI: 10.1063/1.5142470.

[14] Islam Khalil et al. “Self-Assembled Sperm-Templated Micro-Bio-Robots”. 2020.

[15] Islam Khalil et al. “Swimming Back and Forth Using Planar Flagellar Propulsion at Low Reynolds Numbers”. In: *Advanced Science* 1700461 (Dec. 2017), pp. 1–9. DOI: 10.1002/advs.201700461.

[16] Islam Khalil et al. “Three-dimensional closed-loop control of self-propelled microjets”. In: *Applied Physics Letters* 103 (Oct. 2013), pp. 172404–172404. DOI: 10.1063/1.4826141.

[17] Bradley Kratochvil et al. “OctoMag: An Electromagnetic System for 5-DOF Wireless Micromanipulation”. In: *IEEE Transactions on Robotics* 26 (2010), pp. 1006–1017.

[18] Veronika Magdanz et al. “Dynamic Polymeric Microtubes for the Remote-Controlled Capture, Guidance, and Release of Sperm Cells”. In: *Advanced Materials* 28 (Mar. 2016). DOI: 10.1002/adma.201505487.

[19] Veronika Magdanz et al. “IRONSperm: Sperm-templated soft magnetic microrobots”. In: *Science Advances* 6 (July 2020), eaba5855. DOI: 10.1126/sciadv.aba5855.

[20] Veronika Magdanz et al. “Sperm–Particle Interactions and Their Prospects for Charge Mapping”. In: *Advanced Biosystems* (July 2019). DOI: 10.1002/adbi.201900061.

[21] Veronika Magdanz et al. “Spermatozoa as Functional Components of Robotic Microswimmers”. In: *Advanced Materials* 29 (Mar. 2017), p. 1606301. DOI: 10.1002/adma.201606301.

[22] Mariana Medina-Sánchez et al. “Cellular Cargo Delivery: Toward Assisted Fertilization by Sperm-Carrying Micromotors”. In: *Nano Letters* 16 (Dec. 2015). DOI: 10.1021/acs.nanolett.5b04221.

[23] Brad Nelson, Ioannis Kaliakatsos, and Jake Abbott. “Microrobots for Minimally Invasive Medicine”. In: *Annual review of biomedical engineering* 12 (Aug. 2010), pp. 55–85. DOI: 10.1146/annurev-bioeng-010510-103409.

[24] E. M. Purcell. “Life at low Reynolds number”. In: *American Journal of Physics* 45.1 (1977), pp. 3–11. DOI: 10.1119/1.10903.

[25] E. Ramsden. *Hall-effect sensors: Theory and applications.* 2006.

[26] “The Calculation and Measurement of Helmholtz Coil Fields.” In: (Nov. 1994).

[27] Haifeng Xu et al. *Human Spermbots for Cancer-Relevant Drug Delivery.* 2019. arXiv: 1904.12684 [q-bio.CB].

[28] Berk Yesin, Karl Vollmers, and Brad Nelson. “Modeling and Control of Untethered Biomicrorobots in a Fluidic Environment Using Electromagnetic Fields.” In: *I. J. Robotic Res.* 25 (Jan. 2006), pp. 527–536.

[29] Tony Yu, Eric Lauga, and A. Hosoi. “Experimental Investigations of Elastic Tail Propulsion At Low Reynolds Number”. In: *Physics of Fluids* 18 (July 2006). DOI: 10.1063/1.2349585.